

## Ejecting Electrons from Molecular Anions via Shine, Shake/Rattle, and Roll

Published as part of *The Journal of Physical Chemistry virtual special issue "Daniel Neumark Festschrift"*.

Jack Simons\*

Cite This: *J. Phys. Chem. A* 2020, 124, 8778–8797

Read Online

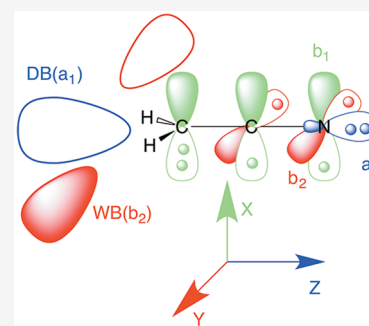
ACCESS |

Metrics &amp; More

Article Recommendations

Supporting Information

**ABSTRACT:** The periodically oscillating electromagnetic potential of a photon can, in an electric-dipole transition, “shine” an electron from an anion’s bound-state orbital directly into a continuum-state orbital. This occurs in photoelectron and photodetachment spectroscopy, both of which provide much information about the electronic structure of the anion. Alternatively, a molecular anion containing sufficient vibrational energy to “shake/rattle” an electron out of a bound-state orbital can induce electron detachment via a vibration-to-electronic nonadiabatic transition. In this case, the electron binding energy in the anion must be smaller than the vibrational energy-level spacing, so these processes involve anion states of low binding energy, and they eject electrons having low kinetic energy. If the anion’s electron binding energy is even smaller, it is possible for a rotation-to-electronic energy transfer to “roll” an electron from the bound-state orbital into the continuum. For each of these mechanisms by which electron detachment can occur, there are different selection rules governing the angular distribution in which the electrons are ejected, and this manuscript discusses these rules, their origins, and their utility when using spectroscopic tools to probe the anion’s electronic structure. Several examples of the shine-, shake/rattle-, and role-ejection of electrons from a range of experimental conditions are discussed as are similarities and differences among the corresponding selection rules. Of special novelty are the effects arising when electron ejection occurs from orbitals having very low electron binding energies and thus large radial extent.



## I. INTRODUCTION

**I.A. Characterizing Angular Distributions of Ejected Electrons.** In 2014, Sanov<sup>1</sup> published an outstanding overview of how experimental measurements of the angular distribution of electrons ejected from molecular anions via photon absorption can be used to gain insights into the anions’ electronic structures and internal dynamics. In 2003, Reid<sup>2</sup> offered an earlier overview of many of the same ideas, and the topic has recently been introduced into the mainstream quantum chemistry toolbox by the Krylov group.<sup>3</sup> The reader is referred to these three articles to gain additional perspective about how such angular distribution data have been used in the hands of experimental and theoretical scientists within the chemistry community.

In the present work, the focus is on electron ejection from a molecular anion by processes involving a combination of energy from a photon and from vibrational and/or rotational motions. After reviewing how angular distributions for electron ejection induced by direct photodetachment are used, I introduce a series of mechanisms that also require the participation of vibration/rotation energy. The use of molecular point group and angular momentum symmetry as well as energy conservation constraints are the tools I use to help understand these mechanisms and how angular distribution information might be useful in these cases.

For one-photon processes involving linearly polarized light, the intensity of electrons ejected in a direction characterized by the vector  $\vec{r}$  is expressed as

$$I(\theta) = a[1 + \beta P_2(\cos \theta)] \quad (1)$$

where  $\theta$  is the angle between  $\vec{r}$  and the polarization vector  $\vec{p}$  of the light

$$P_2(\cos \theta) = \frac{1}{2}[3 \cos^2 \theta - 1] \quad (2)$$

and the parameter  $a$  measures the overall intensity of the ejected electrons. It is convention to characterize the observed angular distribution  $I(\theta)$  in terms of the  $\beta$  value that best fits the experimental data to eq 1. A value of  $\beta$  near  $-1$  fits data with  $I(\theta) \propto \sin^2 \theta$ , while a value near  $+2$  fits data with  $I(\theta) \propto \cos^2 \theta$ ; the former being termed perpendicular electron ejections and the

Received: September 2, 2020

Revised: September 26, 2020

Published: September 26, 2020



latter termed parallel when considering the direction relative to the polarization vector  $\vec{p}$ .

**I.B. When the Anion Is Atomic.** For closed-shell atoms or ions, in 1968, Cooper and Zare showed<sup>4</sup> how to express the  $\beta$  parameter in terms of the  $l$  angular momentum quantum number of the orbital from which the electron is photodetached as expressed in eq 3.

$$\beta = [l(l-1)\chi_{l,l-1}^2 + (l+1)(l+2)\chi_{l,l+1}^2 - 6l(l+1)\chi_{l,l+1}\chi_{l,l-1}\cos(\delta_{l+1} - \delta_{l-1})] / (2l+1)[l\chi_{l,l-1}^2 + (l+1)\chi_{l,l+1}^2] \quad (3)$$

The quantities  $\chi_{l,l\pm 1}$  are radial electric dipole matrix elements between the bound and continuum orbitals connecting the  $l$ -value of the orbital from which the electron is ejected and the  $l \pm 1$  angular momentum of the ejected free electron, and the  $\delta_{l\pm 1}$  are phase shifts that arise from the ejected electron's orbital interacting with the underlying molecule's nuclei and other electrons as well as with its own centrifugal potential. As I discuss later, the magnitudes of these integrals will depend on the radial extent of the orbital from which the electron is detached and on the de Broglie wavelength (reflected in the kinetic energy) of the free-electron orbital.

It is clear from eq 3 that  $\beta$  can assume positive or negative values depending on the sign and magnitude of the  $6l(l+1)\chi_{l,l+1}\chi_{l,l-1}\cos(\delta_{l+1}-\delta_{l-1})$  term that arises from the interference between the ejected electron's orbitals having angular momenta of  $l+1$  and  $l-1$ . For detachment from an s atomic orbital, the ejected electron leaves with  $l=1$  angular momentum in a so-called p-wave, and  $\beta=2.0$  as eq 3 shows (since  $\chi_{l,l-1}$  can be set to 0 for this case). In this case, there is no interference between waves with  $l+1$  and  $l-1$  angular momenta, because there is no  $l-1$  wave.

However, for the detachment from an orbital with nonzero but pure angular momentum, there are three contributions to  $\beta$ :  $\chi_{l,l+1}^2$  arising from ejection into a wave of angular momentum  $l+1$ ,  $\chi_{l,l-1}^2$  from a wave of angular momentum  $l-1$ , and the interference term  $\chi_{l,l+1}\chi_{l,l-1}$ . The sum of the first two (positive) terms and the potentially negative third term can give rise to a somewhat complicated angular distribution in which  $\beta$  can be 0.0, negative, or positive depending on the kinetic energy of the detached electron. For example, in ref 4 it is shown that detachment from a 2p ( $l=1$ ) orbital of the  $O^-$  anion produces free electrons of both s-wave and d-wave character. Near threshold, where the s-wave dominates (because it has no centrifugal barrier to overcome),  $\beta$  turns out to be zero (in eq 3 set  $\chi_{l,l+1}=0$  and retain only  $\chi_{l,l-1}$ ), so the angular distribution is isotropic. However, above the threshold where both the s- and d-waves contribute,  $\beta$  can be quite dependent on the photon energy (as reflected in the kinetic energy of the ejected electrons). In ref 4 a plot of the photon energy dependence of  $\beta$  for the  $O^-$  2p orbital's detachment is shown. In this plot,  $\beta$  begins at zero as noted above, then evolves to negative values (as the negative interference terms in the numerator of eq 3 come into play) approaching  $\beta=-1.0$ , where it reaches its minimum, after which it evolves toward positive  $\beta$  at high photon energies. So, even for atomic ions, the angular dependence of the ejected electrons, although limited to one or two channels, can be somewhat challenging to interpret, because the contributions from competing channels vary differently with energy.

Let us reflect a bit more on the case just described—detachment from a p orbital that generates s- and d-waves. In the

quantum process in which a photon whose electric field vector is polarized along the  $z$ -axis acts on a  $p_z$  orbital, the first-order (in electric field strength) perturbative correction to the wave function is proportional to  $z \otimes p_z$ . Because the  $p_z$  orbital itself has an angular form proportional to  $z$ ,  $z \otimes p_z$  is proportional to  $z^2$ , which can be expressed as  $\frac{r^2}{3}[(3\cos^2\theta-1) + 1]$ . Writing the first-order wave function in this manner illustrates how it is composed of one term whose angular form involves the  $Y_{2,0}(\theta)$  spherical harmonic and one involving  $Y_{0,0}(\theta)$ . These d and s terms are affected differently by the potentials in the molecular Hamiltonian arising from the nuclei, the other electrons, and their respective centrifugal potentials. As a result, when evolved in time and projected onto the asymptotic region describing the electron ejection, the wave function  $\Psi$  becomes a superposition of s and d components that have different amplitudes and differ in phase by  $\exp(i\pi + \delta_2 - \delta_0)$ , where the  $\delta_n$  are phase shifts arising from the influence of the potentials mentioned above. The factor of  $\exp(i\pi)$  is what gives rise to the fact that, when  $|\Psi|^2$  is formed, the s and d contributions each contribute in a positive manner, but their product comes in with a minus sign as in  $|\Psi|^2 = C_0^2 s^2 + C_2^2 d^2 - 2C_0C_2 \cos(\delta_2 - \delta_0)sd$ . For the example considered here, the angular distribution of the ejected electrons depends on the electrons' kinetic energy because the coefficients  $C_n$  do. The first two factors produce isotropic (from the  $s^2$ ) and parallel to  $z$  (from the  $d^2$  which is directed along  $z$ ) ejection, while the negative third term acts to deplete the ejection along  $z$ . It is common in the jargon of photoelectron angular distribution to emphasize that these negative terms arise in  $\beta$  in a manner that can render  $\beta$  negative (see eq 3) thus leading to electron ejection perpendicular to  $z$ . However, it should be clear from this discussion that the effects of these interference terms can alternatively be thought of as reducing the electron flux along  $z$  thus producing a total electron flux that has relatively higher intensity in the  $x,y$  plane, where the isotropic contribution from  $C_0^2 s^2$  remains unaffected by the interference.

**I.C. When the Anion Is Molecular.** For a molecule, the molecular orbital (MO) from which the electron is ejected contains, in general, components of varying angular momentum character often delocalized over several atomic centers. In other words, the MO will be of the form

$$\Psi = \sum_{a,\text{atoms}} \sum_{j,l,m} C_{a;j,l,m} R_{a;j,l}(r_a) Y_{a;l,m}(\theta_a, \phi_a) \quad (4)$$

where the  $R_{a;j,l}(r_a)$  are radial functions centered on the  $a$ th atom,  $Y_{a;l,m}(\theta_a, \phi_a)$  are angular functions centered on this same atom, and the  $C_{a;j,l,m}$  are expansion coefficients. In some molecules, the active MO is highly localized on one atom and has a dominant angular momentum character. For example, in  $OH^-$  the orbital is predominantly an oxygen-centered 2p orbital aligned perpendicular to the bond axis, so it has a predominantly  $l=1$  character. For the dipole-bound orbital in  $ClLi^-$ , the active orbital consists primarily of lithium-centered 2s and 2p <sub>$\sigma$</sub>  orbitals that form an sp-hybrid-like orbital directed away from the Cl atom. For the antibonding  $\pi^*$  orbital in  $O_2^-$  the MO consists primarily of 2p <sub>$\pi$</sub>  orbitals on the two oxygen atoms combined in an out-of-phase manner. In this case, the resulting MO contains a dominant d character, but it is important to note that this does not mean this is a 3d orbital. It is of d angular character, but its radial nature is still determined by the two oxygen 2p orbitals from which it is formed.

It is also important to appreciate that, even when I describe an MO as primarily of a single atomic orbital type, there can be

minor components that can have a significant influence on the angular distribution of an electron ejected from it. Let us consider two examples to illustrate this point. In Figure 1a I

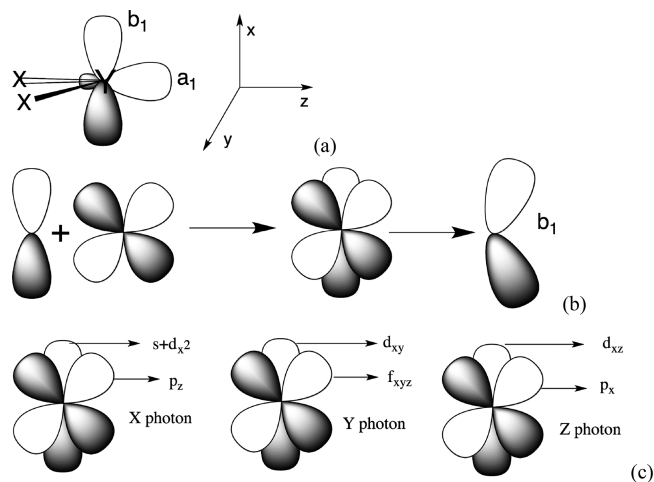


**Figure 1.** Depictions of  $a_1$  and  $b_1$  symmetry molecular orbitals for a molecule  $X_2Y$  in  $C_{2v}$  symmetry and the three Cartesian axes used to label the orbitals (a). In (b) it is shown how the  $b_1$  orbital can be polarized away from the X groups by an admixture of  $d_{b_1} = d_{xz}$  orbital character. In (c) are shown the symmetries resulting from photons aligned along each of the Cartesian axes acting on the  $b_1$  MO's primary ( $p_x$ ) and polarization ( $d_{xz}$ ) components.

show a molecule  $X_2Y$  having  $C_{2v}$  symmetry with an in-plane  $sp^2$ -type hybrid MO of  $a_1$  symmetry and an out-of-plane MO of  $b_1$  symmetry. In describing the photodetachment of an electron from the  $a_1$  MO induced by a photon with polarization aligned along the  $z$ -axis, it is clear that one has to consider this orbital to possess both  $l = 0$  ( $s$ ) and  $l = 1$  ( $p$ ) character. As such, one expects electrons to be ejected in  $s \rightarrow p_z$ ,  $p_z \rightarrow s$ , and  $p_z \rightarrow d_{z^2}$  transitions to generate  $p_z$ -,  $s$ -, and  $d_{z^2}$ -wave free electrons, respectively, with the  $s \rightarrow p_z$  transitions producing a parallel distribution of ejected electrons and the  $p_z \rightarrow s$ , and  $p_z \rightarrow d_{z^2}$  transitions producing isotropic (through the  $s$ -wave), parallel (through the direct contribution of the  $d_{z^2}$ -wave), and perpendicular (through the interference between the  $s$ - and  $d_{z^2}$ -waves) distributions.

When describing the detachment of an electron from the  $b_1$  MO, it is tempting to assume that this orbital contains only  $l = 1$  ( $p$ ) character, so it should generate  $s$ - and  $d$ -wave free electrons. However, this is not the entire story. The nature of the X groups attached to the central Y atom can cause the  $b_1$  orbital to become polarized either away from (e.g., if the X groups produce steric repulsion) or toward (e.g., if the X groups help delocalize the electron) the X groups. In Figure 1b I illustrate how this orbital polarization is introduced in quantum chemistry calculations by allowing the MO to acquire an admixture of  $d_{b_1} = d_{xz}$  orbital character and suggest that this is the more accurate way to view such an orbital. This polarized MO still has purely  $b_1$  symmetry, but now it contains both  $l = 1$  ( $p_z$ ) and (a perhaps minor component of)  $l = 2$  ( $d_{xz}$ ) character (whose radial form will still be similar to its  $l = 1$  component as explained earlier). So electron ejection from this polarized MO would involve  $p \rightarrow s$ ,  $p \rightarrow d$ ,  $d \rightarrow p$ , and  $d \rightarrow f$  transitions and would generate  $s$ -,  $d$ -,  $p$ -, and  $f$ -wave free electrons. Near threshold the various waves'

intensities vary inversely with their  $l$ -value, which governs the centrifugal barrier through which the electron must escape.

In Figure 1c I show the symmetries of the various waves generated by the action of photons polarized along each of the Cartesian axes on the  $p_x$  and  $d_{xz}$  components of the  $b_1$  orbital. To illustrate, when a photon polarized along the  $x$ -axis is used to detach an electron from the  $b_1$  orbital,  $s$ - and  $d_{x^2}$ -waves will be formed from the  $p_x$  component of the  $b_1$  orbital, and a  $p_z$ -wave will be formed from the  $d_{xz}$  polarization component. The  $s$ -wave will dominate at threshold (producing an isotropic distribution), but the  $p_z$ -wave electrons can be expected to contribute as the photon energy increases (contributing a perpendicular distribution) even prior to when the perhaps higher-intensity  $d_{x^2}$ -wave electrons appear (generating perpendicular distribution through their interference with the  $s$ -wave as well as parallel distribution via the  $d_{x^2}$ -wave's direct contribution).

This example serves to illustrate how perpendicular electron ejection can occur via interference between  $s$ - and  $d$ -waves as well as be a result of the orbital from which detachment takes place having a polarization ( $d_{xz}$  in this case) component. Note that, when the  $s$ - and  $d_{x^2}$ -waves interfere to reduce the electron flux along  $x$  as explained earlier, the  $\beta$  parameter becomes negative from interference between the  $s$ - and  $d_{x^2}$ -waves even though the  $d_{x^2}$ -wave itself is directed parallel to the photon's polarization. In contrast, the perpendicular ejection caused by the action of the  $x$ -polarized photon on the  $d_{xz}$  component of the  $b_1$  orbital does not arise from interference; it is simply because the direct product of the photon and orbital symmetries  $x \otimes xz = z$  is perpendicular to the photon's polarization. If the photon had been  $z$ -polarized, perpendicular ejection would still be the result, since  $z \otimes xz = x$  is perpendicular to  $z$ .

While discussing how waves of different symmetry are formed and how they contribute to the angular distribution over various ranges of the ejected electron's kinetic energy (KE), it is worth noting that the exclusion of all but  $s$ -waves at the threshold means that so-called zero kinetic energy experiments<sup>5</sup> (ZEKE) are limited, because they can only probe  $s$ -waves, while the more recent slow electron velocity imaging (SEVI) tools pioneered by Neumark<sup>6</sup> have been successful in probing higher  $l$ -wave contributions as well.

**1.D. What Happens When the Electron Is Ejected from an Orbital of Mixed  $s$ - and  $p$ -Character.** As just illustrated, molecular orbitals often contain a mixture of different  $l$  characters, so the  $\beta$  parameter that characterizes the angular distribution of electrons ejected from molecular anions can be complicated to analyze. In 1976, Reed et al.<sup>7</sup> showed how to use the kind of MO expansion in eq 4 together with the kind of information embodied in eq 3 to express the energy dependence of the photodetachment cross-section for molecular anions in a useful analytical form. In particular, they emphasized how the cross-section depends on the photon energy, which determines the KE of the detached electron. In the quantum chemistry codes used in ref 3 and in the sources cited therein, the full expansion of the active MO as in eq 4 is used, and the near-threshold behavior of the photodetachment cross-section is calculated. The near-threshold behavior has proven to be especially interesting and useful to probe, because, as mentioned above, processes that eject electrons having the lowest accessible angular momentum ( $l_f$  to denote for the free electron) are dominant. The centrifugal barrier  $\frac{l_f(l_f+1)\hbar^2}{2m_e r^2}$  is higher for higher  $l_f$  values, so electrons having the smallest  $l_f$  are most efficient at

tunneling outward and escaping. In 1948, Wigner showed that, near threshold, the cross-section for photodetachment into a free-electron state having an angular momentum value of  $l_f$  varies with the KE of the departing electron as

$$\sigma(\text{KE}) \propto \text{KE}^{(l_f+1/2)} \quad (5)$$

Hence, for so-called s-wave electrons (having  $l_f = 0$ ), the cross-section has a sharp rise at threshold, while, for p- and d-wave electrons, the cross-section has a zero slope at threshold. For an MO having contributions from several  $l$ -values (i.e., as in eq 4), the cross-section will be a sum of contributions from several  $l_f$  waves

$$\sigma(\text{KE}) \propto \sum_{l_f} C_{l_f} \text{KE}^{(l_f+1/2)} \quad (6)$$

In ref 1 Sanov offers a nice description of how the different KE dependences of the various  $l_f$  waves' cross sections give rise to the KE dependence of the  $\beta$  parameter. At threshold,  $\beta$  is dominated by the contribution from the lowest  $l_f$  wave;<sup>2</sup> as KE increases, contributions from higher  $l_f$  waves arise. As demonstrated in ref 1, for the photodetachment of an electron from an MO that is a mixture of s- and p-atomic orbitals

$$\Psi = \sqrt{f}p + \sqrt{1-f}s \quad (7)$$

$\beta$  turns out to depend on KE as follows.

$$\beta = \frac{2Z^*(A^*\text{KE}) + 2(A^*\text{KE})^2 - 4(A^*\text{KE})\cos(\delta_2 - \delta_0)}{1 + 2(A^*\text{KE})^2 + Z^*(A^*\text{KE})} \quad (8)$$

This equation is obtained by starting with the Cooper-Zare result in eq 3 and making use of the Wigner expression in eq 5 to express the KE dependence of the various  $l \rightarrow l \pm 1$  cross sections as was shown by Hanstorp et al.<sup>8</sup> in 1989. Although this result assumes the near-threshold KE dependences of eq 5, it has proven to provide a reasonable description of  $\beta(\text{KE})$  even significantly above threshold.

In eq 8 the parameter  $Z$  depends on the p/s orbital mixing parameter  $f$  as well as on the ratio  $B/A$  whose meaning is explained below.

$$Z = \frac{B}{A} \times \frac{1-f}{f} \quad (9)$$

The quantity  $A^*\text{KE} = \left| \frac{\chi_{i,2}}{\chi_{i,0}} \right|$  involves the ratio of the p  $\rightarrow$  d and p  $\rightarrow$  s electric dipole radial integrals in eq 3, while  $B^*\text{KE} = \frac{\chi_{0,1}^2}{\chi_{i,0}^2}$  involves the ratio of the s  $\rightarrow$  p and p  $\rightarrow$  s integrals.<sup>9</sup> The photon-energy dependence of  $\beta$  is contained in the three  $A^*\text{KE}$  terms in the numerator of eq 8 and the two  $A^*\text{KE}$  terms in the denominator. Some of these terms are positive, some can be negative, and some vary linearly and others quadratically with KE. In ref 11 Sanov shows that, while  $B/A$  does not depend on KE (hence,  $Z$  does not depend on KE under the assumptions made in ref 8), it does depend on the  $n$  quantum number of the s and p orbitals. In ref 11 it is shown that  $B/A$  is 8/3 for 2s/2p orbitals and evolves smoothly as the  $n$  quantum number increases to smaller values approaching 5/3 for Rydberg-like s/p orbitals. For this reason, in our analysis I will assume  $B/A$  to be between 1.6 and 2.6 for photon-induced electron ejection. However, as I show in the Supporting Information, for electron ejection induced by nonadiabatic energy flow from vibrational

or rotational motion, the corresponding  $B/A$  ratio is different but still independent of KE.

From eq 8, one notes that the interference between the s- and d-waves can only cause  $\beta$  to become negative if  $Z < 2.0 - (A^*\text{KE})$ . Assuming that  $B/A$  is 8/3 (see above), this constraint will be met only if the fraction  $f$  of the p-character in the orbital obeys  $f > \frac{8}{14 - 3(A^*\text{KE})} > 4/7$ . I will show examples later of s/p hybrid orbitals in which  $f$  is nonzero yet small enough to have no negative  $\beta$  and other cases where  $f$  is large enough to generate negative  $\beta$ .

Ignoring the d-wave to s-wave phase-difference ( $\delta_2 - \delta_0$ ) (i.e., setting  $\cos(\delta_2 - \delta_0) = 1$  as justified in ref 1) allows eq 8 to be used to plot  $\beta$  as a function of KE as shown in Figure 2 for various

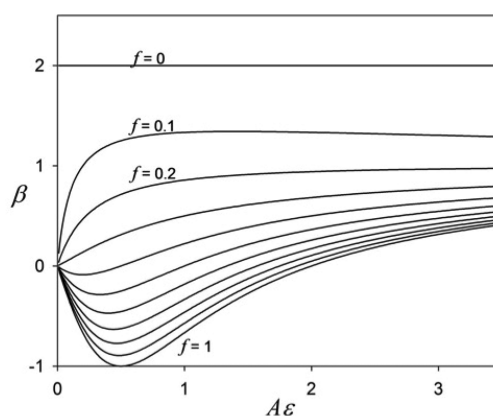


**Figure 2.** Plots of  $\beta$  as a function of  $A^*\text{KE}$  for various values of  $Z$ . Reproduced from ref 10, with the permission of AIP Publishing.

values of the s/p hybrid mixture as reflected in the  $f$  parameter.<sup>10</sup> In this figure, I note that indeed  $\beta$  does not assume negative values for values of  $f$  less than ca. 0.4 and that  $\beta$  reaches its lowest value  $-1.0$  at  $A^*\text{KE} = 0.5$  when  $f = 1.0$ , as eq 8 predicts.

From eq 9 I note that  $f$ -values near zero (large  $Z$ ) describe photodetachment from an MO of dominant s character (as in  $\text{H}^-$ ), which generates ejected electrons in p-waves. In this case, the  $2Z^*(A^*\text{KE})$  terms in the numerator and denominator of eq 9 dominate as long as the photon energy is low enough to guarantee that  $A^*\text{KE} < Z$  so that the  $2(A^*\text{KE})^2$  and  $-4(A^*\text{KE})\cos(\delta_2 - \delta_0)$  terms can be ignored. In this case,  $\beta$  turns out to be  $+2.0$ , once KE is large enough for  $Z^*A^*\text{KE} \gg 1$ , consistent with a parallel distribution of the ejected electrons.

Alternatively, small  $Z$ -values describe detachment from an MO of dominant p character (as in  $\text{O}^-$ ), which generates ejected electrons in s- and d-waves. In this small- $Z$  case,  $\beta$  begins at zero at low KE, characteristic of s-wave ejection, then (if  $f$  exceeds ca. 4/7 as explained earlier) moves toward  $\beta = -1.0$  as KE increases and the  $-4(A^*\text{KE})\cos(\delta_2 - \delta_0)$  term in eq 8 comes into play as the d-wave grows in amplitude, and then  $\beta$  moves toward and into positive values as KE becomes even larger and the  $2(A^*\text{KE})^2$  term becomes more important.

In Figure 3 I illustrate how such data<sup>11</sup> about the KE dependence of  $\beta$  can be used to deduce information about the s/p admixture of the orbital from which the electron is ejected.

One might be tempted to say that the lone-pair  $a_1$ -symmetry orbitals of  $\text{H}_2\text{N}^-$  and  $\text{Cl}_2\text{C}^-$  are similar 2s/2p  $sp^2$  hybrids, but the data say otherwise. For  $\text{H}_2\text{N}^-$ , the active  $a_1$  orbital seems to be of primarily p character (see  $f = 0.96$  in Figure 3), so it generates s- and d-wave electrons with a plot of  $\beta$  versus KE much like that

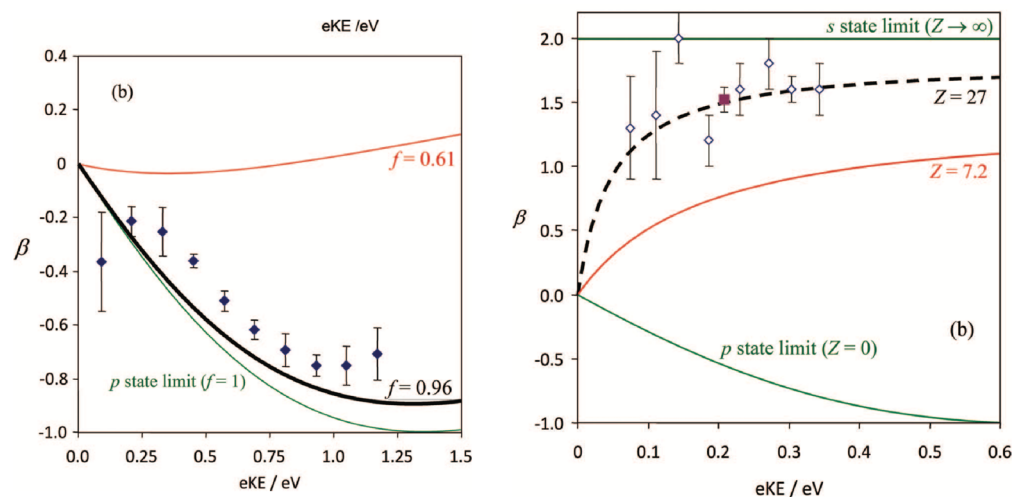


**Figure 3.** Plots of the energy dependence of the  $\beta$  parameter for detaching an electron from the nominal  $sp^2 a_1$  lone-pair orbital of  $H_2N^-$  (left) and  $Cl_2C^-$  (right). Reproduced from ref 11, with the permission of AIP Publishing.

shown at the bottom of Figure 2. In contrast, for  $Cl_2C^-$ , the active  $a_1$  orbital seems to be of primarily  $s$  character as a result of which its plot looks much like those at the top of Figure 2. In ref 11 the authors explain how in-plane  $3p$  orbitals on the two Cl atoms act to influence the  $2s/2p$  admixture in  $Cl_2C^-$ . For our purposes, this example serves to show how the KE dependence of the angular distribution of electron ejection can be useful in interpreting the electronic structures of molecular anions.

It is worth noting that in eq (30) of ref 11 an analytical approximation is given for how the  $A$  parameter depends on the radial extent of the  $2p$  orbital from which the electron is ejected. Assuming that a  $2p$  orbital's asymptotic radial dependence is of the form  $r \exp(-\xi r/2)$ , the authors of ref 11 derive the following expression for  $A$ .

$$A = \frac{16}{\xi^2} \text{Ha}^{-1} = \frac{0.588}{\xi^2} \text{eV}^{-1} \quad (10)$$

The asymptotic form of an  $n-p$  orbital can be approximated as  $r^{n-1} \exp(-[\sqrt{2BE}]r)$ , where BE is the electron binding energy (in Hartree units, Ha) for the orbital in question. So, eq 10 can be rewritten in terms of the orbital's BE as

$$A = \frac{0.0667(n+4)(n+3)}{BE} \text{eV}^{-1} \quad (11)$$

where now BE is given in electronvolts units; for  $n = 2$  orbitals, this equation reads  $A = \frac{2.0}{BE} \text{eV}^{-1}$ .

This result suggests that, for states having extremely small BE values, the  $A$  factor entering into the expression for  $\beta$  could be much larger than the values<sup>11</sup> of 0.37 and 0.75  $\text{eV}^{-1}$  for  $NH_2^-$  and  $CCl_2^-$ , respectively. For example, for a dipole-bound orbital formed from  $2s$  and  $2p_\sigma$  atomic orbitals, BE could be ca. 100  $\text{cm}^{-1} = 0.012 \text{ eV}$ . In such a case, eq 11 suggests that  $A$  will be ca. 160  $\text{eV}^{-1}$ . This, in turn, can cause  $\beta$  to display various KE variations depending on the  $p/s$  orbital ratio in the DBS orbital, as I analyze in the Supporting Information. Also, later I will offer a concrete example from the recent literature of how large  $A$  factors can give rise to unexpected behavior in the KE dependence of the photoelectron angular distribution. In that example, the anion's excess electron density is spread over many atomic centers yet still retains enough overall symmetry to be described as globally  $s/p$ -like. As I will demonstrate, the  $A$  factor

in such cases is likely even larger than suggested by eq 11, whose derivation assumed the diffuse electron density to reside on a single center.

Although the examples shown thus far relate to electron detachment processes that are induced purely by electric dipole photon absorption, I expect that some lessons have been learned or refreshed and will be useful as I now move on to discuss processes that also involve vibration/rotation motion. It is especially important to note that the electric-dipole integrals that arise in the situations discussed thus far are not the same as the integrals that arise when vibration- or rotation-induced nonadiabatic processes are at work, even though much of the symmetry analyses in the two cases are similar.

**I.E. Emphasis in This Work.** In the present work, I will have little if anything to say about the  $\delta$  phase shifts of eq 3. Nor will I discuss how to efficiently compute the photodetachment cross sections using ab initio tools as detailed in ref 3. Instead, I will focus on the roles played by molecular symmetry and size as well as angular momentum and energy conservation in determining  $\beta$ , with discussion also being devoted to the KE dependence of  $\beta$  when molecular vibration/rotation is active. In particular, I will study how the symmetries of the anion's active orbitals (i.e., those occupied by the electron to be ejected) and of the vibrational modes and of rotational degrees of freedom affect  $\beta$  and thus the angular distribution of the ejected electrons. In so doing, I will explore several mechanisms by which the photon absorption process can generate free electrons and will show that different mechanisms produce different angular distributions. I will also show that different mechanisms give different distributions for the KEs of the ejected electrons. This means that experimental observations of angular distributions and KE values can be used to probe the mechanistic process by which the electrons are ejected, and several examples will be used to illustrate this as well as to suggest future experiments that could offer new insights.

## II. THE ANION USED TO ILLUSTRATE VARIOUS PROCESSES BY WHICH ELECTRONS ARE DETACHED

I chose to use the anion formed by deprotonating acetonitrile for the case study partly because this anion has a low-energy valence-bound state as well as a dipole-bound state (DBS)

whose energy lies slightly below that of the neutral's ground state and whose geometry is similar to that of the neutral molecule's ground state. This choice was also made because this anion has several point group symmetry elements that can be used to label its orbitals, vibrational modes, and rotational motions and because it has been extensively studied using a variety of experimental techniques some of which I will discuss here.

Although  $\text{H}_2\text{CCN}^-$  has only one weakly bound state (at least that has been discovered to date), I introduce the possibility that other molecular anions will be discovered that possess more than one such state. For example, a molecule might have a large-enough dipole moment to support both  $\sigma$ - and  $\pi$ -symmetry DBSs, or it might have both a large dipole moment and a large quadrupole moment or polarizability that would allow it to support both a  $\sigma$ -symmetry DBS and a quadrupole- or polarization-bound state. To include such possibilities in our analysis, I assume that our case-study anion has both the  $\sigma$ -symmetry DBS as well as another weakly bound state (WBS) whose symmetry is  $b_2$  in the  $C_{2v}$  point group. As I illustrate later, by considering the possible existence of more than one WBS, I am able to suggest how electron-ejection experimental probes might be used to search for such WBS thus proposing yet-to-be achieved experimental goals.

In Figure 4 I show the  $\text{H}_2\text{CCN}^-$  anion with its active orbitals occupied as in its  $^1A_1$  ground state, and I introduce the  $C_{2v}$  point

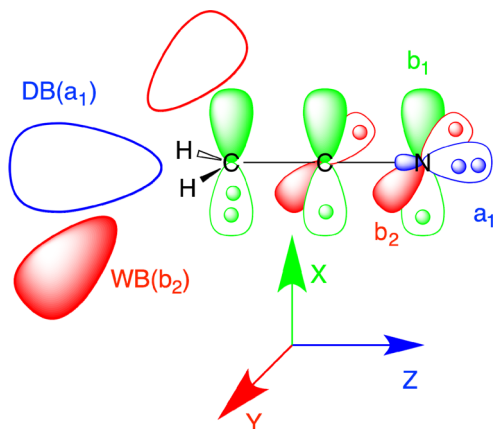


**Figure 4.**  $\text{H}_2\text{CCN}^-$  anion with valence electrons (dots) occupying the  $a_1$  nitrogen lone pair and CCN  $b_1$  and  $b_2$   $\pi$  orbitals along with depictions of one DBO of  $a_1$  symmetry and a hypothetical WBO of  $b_2$  symmetry.

group symmetry labels for these orbitals and for the molecule-fixed Cartesian directions  $x$ ,  $y$ , and  $z$ .

In Figure 5 I show qualitative depictions of the Born–Oppenheimer energy surfaces of

- the anion's  $^1A_1$  ground state.
- the  $^1A_2$  state of the anion formed by promoting one electron from a  $b_1$   $\pi$ -orbital into the hypothetical WBO of  $b_2$  symmetry.
- the  $^1B_1$  state of the anion formed by promoting an electron from a  $b_1$   $\pi$ -orbital into the DBO of  $a_1$  symmetry.
- the  $^2B_1$  state of the neutral formed by removing an electron from a  $b_1$   $\pi$ -orbital.

In 1987, Lykke et al.<sup>12</sup> studied the photodetachment of  $\text{H}_2\text{CCN}^-$  and determined that the  $^2B_1$  state of the neutral lies ca.  $12\,500\text{ cm}^{-1}$  above the  $^1A_1$  ground state of the anion and that the DBS of the anion lies ca.  $60\text{ cm}^{-1}$  below the  $^2B_1$  state of the

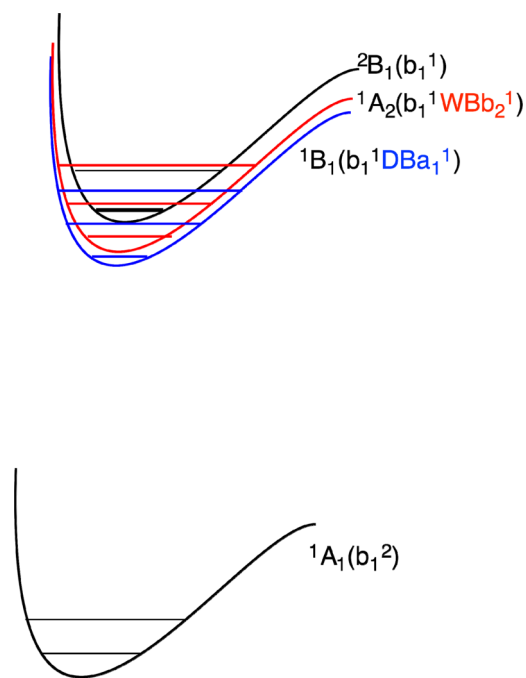


**Figure 5.** Qualitative depictions of the  $^1A_1$  ground state Born–Oppenheimer energy surface of the  $\text{H}_2\text{CCN}^-$  anion (lower black) and of the  $^2B_1$  ground state of the  $\text{H}_2\text{CCN}$  neutral (upper black) formed by removal of an electron from the anion's highest occupied  $b_1$   $\pi$ -orbital. In blue and red are shown depictions of the excited anion states formed by adding one electron to the  $^2B_1$  neutral into either the  $a_1$ -symmetry DBO or the hypothetical  $b_2$ -symmetry WBO illustrated in Figure 4.

neutral. So, the spacings among the four states shown in Figure 4 are distorted (to make the figure easier to view); the DBS and WBS are very close in energy and geometry to the  $^2B_1$  neutral, and the  $^1A_1$  state of the anion is far below. These energy-gap magnitudes are important to keep in mind, because they relate to the kind of spectroscopies used to probe the various mechanisms I will discuss here. For example, using one photon to directly detach an electron from a  $b_1$   $\pi$ -orbital to leave the neutral in some vibration/rotation state of the  $^2B_1$  electronic state would require a light source in the  $12\,500\text{ cm}^{-1}$  range or higher and would involve an electronic transition. In contrast, to detach an electron from the  $^1B_1$  DBS of the anion one could use an IR or far-IR light source, and two outcomes would be possible: (i) the electron could be directly detached from the  $a_1$  DBS orbital in an electric-dipole induced transition or (ii) the photon could be absorbed to generate an excited vibration/rotation state of the DBS, after which a nonadiabatic transition could eject the electron from the  $a_1$  DBS orbital. I will discuss later what happens in each of these situations (and more).

### III. SEVERAL MECHANISMS FOR ELECTRON EJECTION

**III.A. Shine: The Direct One-Photon Electric-Dipole Detachment Process.** In Figure 6 I illustrate the nonresonant process in which photons of fixed energy detach an electron from a specific orbital (the highest-occupied  $b_1$  MO in this example) to generate free electrons whose kinetic energies and numbers are then measured and whose angular distributions are examined. The kinetic energy of the ejected electron will depend on which vibrational level of the neutral is formed in the detachment and on the energy of the photon.

This direct detachment is dipole-allowed (as elaborated upon below) and results in electrons being ejected

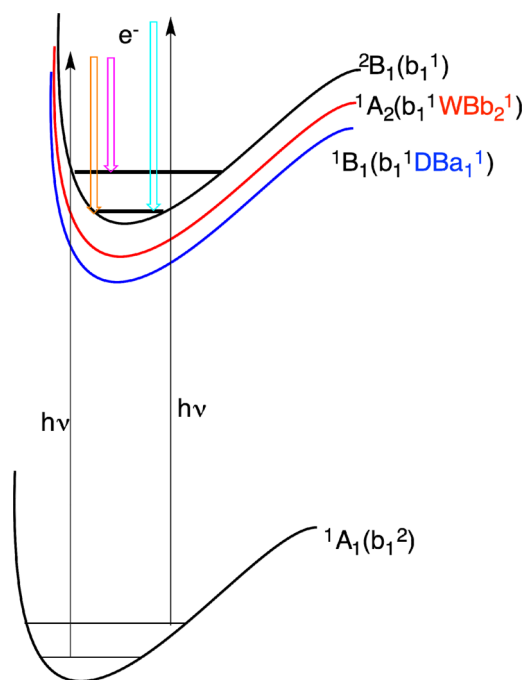


**Figure 6.** Illustration of  $\nu = 0$  (orange),  $\nu = 1$  (magenta), and  $\nu = 0$  hot band (aqua) nonresonant transitions involved in direct photodetachment from the  ${}^1A_1$  ground state of the anion to the  ${}^2B_1$  ground state of the neutral. The photon's energy is shown as the black arrows, and the kinetic energies of the ejected electrons are depicted as downward-directed colored arrows whose lengths relate to the KE values.

- a. with KE equal to the photon energy  $h\nu$  minus the  ${}^2B_1$ -to- ${}^1A_1$  energy gap (the electron affinity EA) minus any vibrational energy ( $E_{\text{vib}}$ ) deposited into the  ${}^2B_1$  neutral and, for hot bands, any vibrational energy removed from the  ${}^1A_1$  ground state.

$$\text{KE} = h\nu - \text{EA} - E_{\text{vib}} \quad (12)$$

- b. with an angular distribution governed by the direct product of the  $b_1$  symmetry of the orbital from which the electron is ejected and the polarization of the laser's photons in addition to which
- c. the symmetry of any vibrational modes excited or, for hot bands, de-excited must be also taken into consideration.

To illustrate, a transition from the lowest vibrational level of the ground-state anion that detaches an electron from the  $b_1$  orbital and leaves the neutral in the  $\nu = 1$  level of the out-of-plane  $b_1$  vibration of the  $\text{H}_2\text{C}^-$  group would be treated as follows:

- The symmetry of the orbital from which the electron is ejected is  $b_1$ , and there are no vibrations in the ground-state anion that are excited, so they add no more to the initial symmetry.
- The final state involves an ejected electron whose symmetry I wish to determine and one quantum of vibration in the  $b_1$  mode.
- So, the direct product of the symmetry of the photon times that of the initial orbital ( $b_1$ ) must match the direct product of the symmetry of the ejected electron times that of the excited vibration ( $b_1$ ):  $\text{symmetry}_{\text{photon}} \otimes \text{symmetry}_{\text{orbital}} = \text{symmetry}_{\text{electron}} \otimes \text{symmetry}_{\text{vibration}}$ . This means that the electron will be ejected with the same symmetry as the photon that ejected it in this case. In

other words, the electron will be ejected parallel to the photon's polarization.

In contrast, a transition that ejects the electron from the  $b_1$  orbital and excites a vibration of  $a_1$  symmetry will eject electrons in waves of  $a_1$  symmetry if the photon's polarization is along  $x$  ( $b_1$ ) or waves of  $b_1$  symmetry if the photon's polarization is along  $z$  ( $a_1$ ). In this case the electrons will be ejected perpendicular to the photon's polarization.

Actually, things are a bit more complicated, because, when considering the angular momentum character of this  $b_1$  orbital, it is important to keep in mind what I emphasized earlier. This orbital is not a purely carbon  $2p_x$  orbital; it is polarized by the nearby groups and thus contains a  $d_{xz}$  component. For this component, an  $x$ -polarized photon will generate a  $p_z$  wave, while a  $z$ -polarized photon will produce a  $p_x$  wave, in both cases contributing to a perpendicular electron ejection.

In Table 1 I summarize the symmetries in which electrons are ejected from orbitals of  $a_1$  ( $s$  or  $p_z$  or  $sp$  hybrid as in our

**Table 1.**  $C_{2v}$  Point Group Symmetries<sup>a</sup>

$\vec{p}$ vector	$a_1^{-1}(s)$	$a_1^{-1}(p)$	$b_1^{-1}(p)$	$b_2^{-1}(p)$
$z(a_1)$	$a_1(p_z)$ 	$a_1(s) + a_1(d_z^2)$ O,   , I( $\perp$ )	$b_1(p_x) * b_1(d_{xz})$ $\perp^*$	$b_2(p_y) * b_2(d_{yz})$ $\perp^*$
$x(b_1)$	$b_1(p_x)$ 	$b_1(d_{xz})$	$a_1(s) + a_1(d_x^2)$ O,   , I( $\perp$ ) $a_1(p_z)^*$ $\perp^*$	$a_2(d_{xy})$
$y(b_2)$	$b_2(p_y)$ 	$b_2(d_{yz})$	$a_2(d_{xy})$	$a_1(s) + a_1(d_{y^2})$ O,   , I( $\perp$ ) $a_1(p_z)^*$ $\perp^*$

<sup>a</sup> $C_{2v}$  point group symmetries and s-, p-, or d-wave character of electrons ejected using single-photon absorption having linear polarization along any of the three Cartesian axes. The symbols || and  $\perp$  denote electrons ejected parallel or perpendicular to the photons' polarization  $\vec{p}$ , respectively; O is used to denote isotropic ejection, and I( $\perp$ ) specifies that interference between s- and d-waves is present and will produce perpendicular electron ejection. The (\*) symbol identifies components resulting from the d-orbital polarization character as illustrated in Figure 1.

example),  $b_1$  ( $p_x$  with polarization from  $d_{xz}$  in our example), or  $b_2$  ( $p_y$  in our example<sup>13</sup>) symmetry using laser light of  $z$ ,  $x$ , or  $y$  polarization (see Figure 4). The symmetries of the ejected electron waves are arrived at by taking the direct product of the polarization's symmetry and the symmetry of the orbital from which the electron is removed (keeping in mind that the orbital can have a polarization component as well) and then decomposing this product into s, p, and d elements. For example, a  $z$ -symmetry photon combined with a  $p_z$  orbital will generate a function proportional to  $z^2$ , which can be decomposed into an s component ( $r^2$ ) and a d component (as in  $d_z^2$ ). This is an example of what I said earlier about how electron ejection from an orbital of nonzero  $l$ -value generates waves having angular momenta of one higher and one lower  $l$ -value.

In the example just discussed (ejection from a  $p_z$  orbital by a photon of  $z$  polarization), such an electron ejection would produce a partial isotropic (from the s-wave) and a partial parallel (since the  $d_z^2$  orbital has its major lobes directed along the  $z$  axis) electron ejection. However, the d-wave contributes to

$\beta$ 's sign in two terms,  $+2(A^*KE)^2$ , which arises from its direct contribution, and  $-4(A^*KE)\cos(\delta_2-\delta_0)$ , which comes from the interference between the  $d_{z^2}$ - and  $s$ -waves. At lower KE, the negative term dominates and can make  $\beta$  negative (if  $f$  is large enough as explained earlier), as a result of which the total intensity of the ejected electrons is predominantly perpendicular to the laser's polarization at such energies. At higher KE the positive term  $+2(A^*KE)^2$  can become dominant and make  $\beta$  positive. This example illustrates that, when contemplating the overall angular distribution of ejected electrons, it is important to keep in mind both the direction (i.e., parallel or perpendicular) of each ejected wave as well as the fact that  $s$ - and  $d$ -waves also contribute interference terms that have effects on the sign of  $\beta$ .

In Table 1 I do not assign parallel or perpendicular labels to the  $d_{xz}$ ,  $d_{yz}$ , or  $d_{xy}$  waves, because, as noted in ref 10, the value of  $\beta$  can be determined from the electron-ejection intensity  $I(\theta)$  at  $\theta = 0^\circ$  and at  $\theta = 90^\circ$ . Because  $d_{xz}$  and  $d_{yz}$  vanish at such angles (defined relative to the  $z$ -axis);  $d_{xz}$  and  $d_{xy}$  vanish at such angles (defined relative to the  $x$ -axis); and  $d_{xy}$  and  $d_{yz}$  vanish at such angles (defined relative to the  $y$ -axis), they can be ignored when determining  $\beta$ .

When making use of the symmetry relations in Table 1, it is important to keep in mind that, whenever  $s$ - and  $d$ -waves are generated in the same photon-absorption event, there will also be a potentially negative contribution to  $\beta$  arising from the interference between these two waves. As explained earlier, this can happen only if the orbital from which the electron is detached has a fraction of  $p$  character exceeding ca.  $4/7$  (for  $n = 2$  orbitals). For example (see column 3 in Table 1), when  $s$ - and  $d_{z^2}$ -waves are generated, although the  $d_{z^2}$  wave's direct contribution to the angular distribution of ejected electrons is along the  $z$ -axis (thus labeled  $\parallel$  in Table 1), the interference between these two waves can cause  $\beta$  to become negative corresponding to electrons ejected perpendicular to the photon's polarization (as indicated in the  $I(\perp)$  notation in Table 1). Likewise, when  $s$ - and  $d_{x^2}$ -waves are generated (see column 4 in Table 1), although the  $d_{x^2}$  wave's direct contribution to the angular distribution of ejected electrons is along the  $x$ -axis (thus labeled  $\parallel$  in Table 1), the interference between these two waves can cause  $\beta$  to become negative corresponding to electrons ejected perpendicular to the photon's polarization. So, the  $\parallel$  labels in Table 1, when applied to  $d$ -wave ejection, describe only the direction of the electrons ejected by the direct action of the  $d$  wave; the interference term's influence will be perpendicular to the direct action's ejection (as indicated by  $I(\perp)$ ).

As noted earlier, close to thresholds, when considering the behavior of the photoejected electrons, it is possible to focus on either  $l' = 0$  ( $s$ -wave) or  $l' = 1$  ( $p$ -wave) angular distributions, because the centrifugal potential  $\frac{l'(l'+1)\hbar^2}{2m_e r^2}$  attenuates ejection into higher  $l'$  values. Of course, as also noted earlier, at higher KE, the  $d$ -wave electrons also contribute. These  $l'$ -dependences arise from the well-known<sup>14</sup> near-threshold photoejection cross-section's  $\sigma(E) \propto KE^{l'+1/2}$  dependence of on the ejected electron's KE and  $l'$ -value. Thus, for completeness I also list in Table 1 the ejected electrons' distributions of  $l' = 2$  ( $d$ -wave) character when they too could occur.

In the one-photon electric-dipole photodetachment events being discussed, the electronic transition combined with the symmetries of any vibrational modes that change in the

transition determines the symmetry and thus the angular distribution of the ejected electrons as explained above. The intensities of vibrational features seen in the spectra are also governed by Franck–Condon factors connecting the vibrational levels of the anion and those of the neutral.

Of course, the examples considered thus far are likely well-known to researchers studying photodetachment and photoionization. However, the next mechanisms to be illustrated will hopefully contain new insights that will be of use to workers in the field.

**III.B. Resonance-Enhanced One-Photon Detachment Mediated by Nonadiabatic Vibration/Rotation-to-Electronic Energy Transfer.** *III.B.1. Shake/Rattle: Vibration as the Active Motion.* In this example, I consider using photons whose energy is more than enough to detach an electron and produce the  $^2B_1$  neutral and is resonant with the energy required to excite the anion from its  $^1A_1$  ground state into its excited  $^1B_1$  DBS and, specifically, into an excited vibrational level of the DBS whose total energy lies above one or more vibrational levels of the  $^2B_1$  neutral. For simplicity to illustrate, I consider using photons that produce the  $^1B_1$  DBS in the  $\nu = 1$  level of some mode (call it Q) that places the anion above the energy of Q's  $\nu = 0$  level of the  $^2B_1$  neutral as shown in Figure 7.

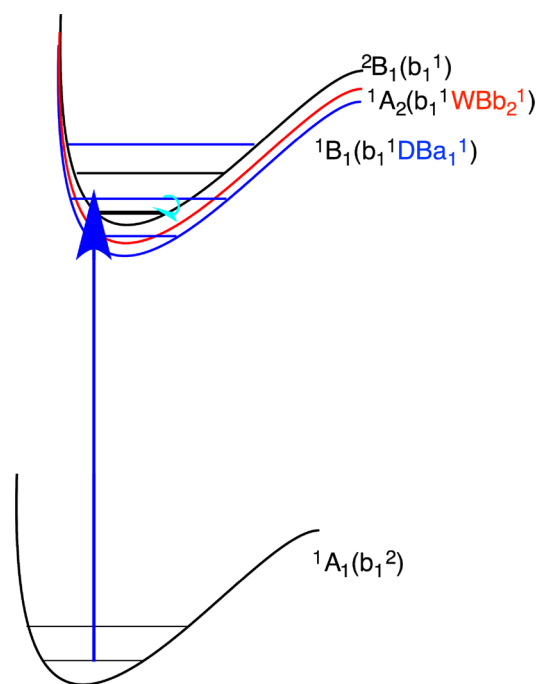


**Figure 7.** Depiction of an electron detachment event involving resonant excitation to the  $^1B_1(b_1,1)DBA_1,1$  state with one quantum of vibrational excitation in some mode followed by a nonadiabatic vibration-to-electronic energy flow (denoted by the curved aqua arrow) from the  $\nu = 1$  level of the  $^1B_1$  anion to the  $\nu = 0$  level of the  $^2B_1$  neutral plus an ejected electron.

In the first step of this transition, promotion of the electron from the ground-state anion's  $b_1$   $\pi$ -orbital into the  $a_1$  DBS orbital requires that the laser photon have  $x$  ( $b_1$ ) symmetry as long as the vibrational level populated in the DBS is of  $a_1$  symmetry. In practice this means that molecules aligned with their  $x$ -axis parallel to the laser's polarization will be able to experience the excitation. The intensity of such resonant excitation will depend on conventional Franck–Condon factors connecting the

vibrational levels of the  $^1A_1$  anion's ground state to the levels of the  $^2B_1$  neutral (because the vibrational modes of the DB state will be very similar to those of the  $^2B_1$  neutral). In Figure 7 I show resonant excitation from a photon whose energy is close to the  $\nu = 1$  level of some mode of the DBS, which is above the  $\nu = 0$  level (i.e., vibrational ground state) of the same mode of the neutral molecule.

With the active electron now in the  $a_1$  DBS orbital, the angular distribution of the electron ejected in the second (nonadiabatic) step is determined by the direct product of the DBS orbital's symmetry and the symmetry of the vibrational mode of the excited anion that promotes the electron detachment. For a vibration of  $a_1$  symmetry, its action on the  $a_1$  DBS orbital involves an operator  $^{15}\nabla_{a_1}$  that has the same symmetry (including parity) as a  $p_\sigma$  orbital. Acting on the DBS orbital of mixed  $s/p_\sigma$  character, this operator generates waves of  $(p_\sigma)x(p_\sigma) = s + d_\sigma = s + d_{z^2}$  and  $(p_\sigma)x(s) = p_\sigma = p_z$  symmetry if the molecule's symmetry axis were directed along  $z$  (if the molecule were aligned along  $y$ , the waves would be  $(p_\sigma)x(p_\sigma) = s + d_\sigma = s + d_{y^2}$  and  $(p_\sigma)x(s) = p_\sigma = p_y$ ). If this detachment takes place before the  $^2B_1$  DBS anion has time to significantly rotate (e.g., within ca.  $10^{-12}$  s), this ejection direction can be connected to the orientation of the laser's polarization. In the example just discussed, the light was polarized along  $x$  ( $b_1$ ), and if the molecule were aligned along  $z$ , the electrons will be ejected isotropically (by the  $s$ -wave), perpendicular (by the  $p_z$  wave), and parallel (by interference between the  $s$  and  $d_{z^2}$  waves) relative to the photon's polarization. However, the relative intensities of these waves depend on the fractional  $p$  character (i.e., the  $f$  parameter) in the DBS orbital. I illustrated earlier how the  $p$  character of nominal  $sp^2$  hybrid orbitals in  $H_2N^-$  and  $Cl_2C^-$  was quite different. In the case of DBS orbitals, it is unlikely that the fraction  $f$  of the  $p$  character will exceed the ca. 4/7 value introduced earlier, as most of the DBS orbitals this author has seen to date have substantially more  $s$  character than  $p$  character. For this reason, it is most likely that the nonadiabatic induced electron ejection will be dominated by the  $p_\sigma = p_z$ -wave arising from the dominant  $s$  component of the DBS orbital, which would be perpendicular to the  $x$ -axis photon in this case.

In the Supporting Information, a detailed analysis of the symmetries and intensities involved in these nonadiabatic processes is given with regard to how the angular distributions I am discussing here, which are described in the molecule-fixed coordinate system, reflect back into the laboratory-fixed coordinates. Although the existence of waves of various angular momenta appears to complicate the situation, there is one factor that acts to simplify things. In these nonadiabatic electron ejection events, the KEs of the ejected electrons will be small, so it is likely that waves having the smallest angular momenta will dominate.

As another example, consider the possibility that the initial excitation populated the  $\nu = 1$  level of an out-of-plane  $b_1$  ( $x$ ) vibrational mode of the DBS with the molecule aligned along the  $z$ -axis. This would require a photon of  $z$  ( $a_1$ ) polarization to excite the electron from the  $b_1$  orbital to the  $a_1$  DBS orbital and simultaneously populate the  $b_1$  vibration in the  $\nu = 1$  level of the DBS. Once the electron is in the DBS orbital, the nonadiabatic ejection induced by the  $b_1$  vibration, which involves the  $\nabla_{b_1}$  operator, acting on the  $s$ -orbital component of the DBS orbital will eject electrons in waves of  $b_1$  (i.e.,  $p_x$ ) symmetry thus perpendicular to the photon's polarization. The DBS orbital also

contains (a likely small amount of)  $p_z$  character, and the action of  $\nabla_{b_1}$  on that generates a wave of  $d_{xz}$  character. However, as explained in the Supporting Information and under Table 1, these off-axis  $d$ -wave terms do not contribute to  $\beta$ . The net result is that electrons will be ejected perpendicular to the photon's  $z$  ( $a_1$ ) polarization in this case.

To summarize how vibrations of different symmetry act to eject electrons from a DBS orbital of mixed  $s$  and  $p_\sigma$  character in such a nonadiabatic process I again make use of Table 1 assuming the molecule to be aligned as in Figure 4.

- A vibration of  $a_1$  symmetry (e.g., the HCH symmetric stretch or C–C–N symmetric stretch) could eject electrons of  $a_1$  ( $s$ ,  $p_\sigma = p_z$  and  $d_\sigma = d_{z^2}$ ) symmetry, but interference between the  $s$  and  $d_{z^2}$  waves would only be strong enough to produce intensity perpendicular to the  $z$ -axis if the fractional  $p_z$  character in the DBS exceeds ca. 4/7, which is not likely for DBS orbitals.
- A vibration of  $b_1$  symmetry (e.g., the HCH out-of-plane mode) could eject electrons of  $b_1$  ( $p_x$ ) symmetry because of the small  $p$ -orbital component of the DBS.
- A vibration of  $b_2$  symmetry (e.g., the HCH asymmetric stretch) could eject electrons of  $b_2$  ( $p_y$ ) symmetry because of the small  $p$ -orbital component of the DBS.

Of course, each of these vibration-induced electron ejections would be expected to involve "downward" vibrational transitions following the  $\Delta\nu = -1$  selection rule, which was shown earlier<sup>16</sup> to apply to such nonadiabatic vibration-to-electronic energy flow processes. Moreover, the rate of such a nonadiabatic process will depend on the strength with which the active vibration modulates the electron binding energy of the  $a_1$  DBS orbital;<sup>16</sup> vibrations that do not substantially affect this orbital will not be effective in electron ejection. For DBS cases, this means that infrared active vibrations are most effective, because they modulate the system's dipole moment, which, in turn, modulates the electron binding energy.

There are two additional features arising in these shake/rattle-derived processes that are worth noting. The kinetic energy of the ejected electrons equals the energy gap between the  $\nu = 1$  level of the DBS and the  $\nu = 0$  (for the active vibrational mode) level of the  $^2B_1$  neutral, which, of course, is equal to the energy in one quantum of the vibration minus the DBS electron binding energy. Because such kinetic energies are most likely to be small, the angular distribution of ejected electrons in these cases is characterized more by the small-KE range of  $\beta$  than in the photon-induced detachment processes discussed earlier. Also, as shown in the Supporting Information, while the functional form for how  $\beta$  varies with KE is the same in the shake/rattle and shine cases, the magnitudes of the  $A$  and  $B$  parameters and of the  $B/A$  ratio differ in the two processes. Of particular note is the fact that the small BE values arising in the former cases (see eq 11 and the Supporting Information) cause  $A$  and  $B$  to be much larger than in the photon-induced electron ejection involving anions having larger BEs. Also, the  $B/A$  ratio for the shake-rattle case is a bit smaller than in the photon-absorption (shine) case. To emphasize the differences between electron ejection (by shine or shake/rattle) from a valence-bound (VB) anion having a BE in the 1 eV range and a DBS anion with a BE near  $100\text{ cm}^{-1}$ , take note of the three factors entering into the numerator of eq 8:  $2Z^*(A^*KE)$ ,  $2(A^*KE)^2$ , and  $-4(A^*KE)\cos(\delta_2 - \delta_0)$ . For the VB system, the  $A$  factor will be ca.  $2\text{ eV}^{-1}$  (see eq 11), while for the DBS  $A$  will be ca.  $160\text{ eV}^{-1}$ . For the factor  $2(A^*KE)^2$ , which varies quadratically with KE, to become as large in magnitude as

the two factors varying linearly,  $A^*KE$  has to approach or exceed 1.0. For the VB system, this requires that the ejected electrons have KEs in the 1 eV range, while for DBS systems, the KE need exceed only ca. 0.01 eV. For a photon-induced ejection process in a DBS system, such KEs are easily accessed. However, in a shake/rattle electron ejection of a DBS system, the KEs can be above or below 0.01 eV. This analysis should make it clear how the angular distributions in VB and DBS species may or may not display similar KE dependences and that the similarity will also depend on whether shine or shake/rattle is operative.

Let us now illustrate how the resonance-enhanced and nonresonant methods just discussed have been employed using recent experimental data from 2013 by Liu et al.<sup>17</sup> involving the phenoxide anion  $C_6H_5O^-$ , which has the same symmetry as the  $H_2CCN^-$  ion I have been using in our examples. In those experiments the workers observed, albeit with higher resolution, many photodetachment features that the Neumark group had already seen<sup>18</sup> in 2011. In the 2013 experiments, when the laser's energy was tuned to populate, for example,  $\nu = 1$  of a specific mode (I will discuss the  $a_1$  symmetry mode 11 and the  $b_1$  symmetry mode 18) of the DBS as in the resonance-enhanced mode, electrons were ejected with KEs equal to the energy of the photon minus the energy of the neutral molecule having  $\nu = 0$  in the excited mode (see Figures 2 and 4 in ref 17). Using the same kind of analysis as I used earlier for  $H_2CCN^-$ , one would expect that (assuming the anion to have its  $C_{2v}$  symmetry axis directed along  $z$  and its  $b_1$  orbital directed along  $x$ )

- (i) when 538 nm photons were used to resonantly promote the  $b_1$  (oxygen  $2p_x$ ) electron into the  $a_1$  DBS orbital and populate the  $\nu = 1$  level of the  $a_1$  mode 11 of the DBS,  $x$  ( $b_1$ ) photons were involved, and subsequently the  $a_1$  mode 11 vibration was able to eject electrons in an  $a_1$  ( $p_z$ ) perpendicular wave from the  $s$  component of the DBS, and  $s$  and  $d_{z^2}$  from the  $p_z$  component of the DBS with the  $s$ -wave producing isotropic ejection and interference between the  $s$  and  $d_{z^2}$  waves generating intensity parallel to the  $x$ -axis photon (as well as along the  $y$ -axis) through interference but only if the fraction ( $f$ ) of  $p$  character in the DBS exceeds ca. 4/7 as explained earlier.
- (ii) when 534 nm photons were used to resonantly promote the  $b_1$  (oxygen  $2p_x$ ) electron into the  $a_1$  DBS orbital and populate the  $\nu = 1$  level of the  $b_1$  mode 18 of the DBS,  $z$  ( $a_1$ ) photons were involved, and subsequently the  $b_1$  mode-18 vibration was able to eject electrons in a  $b_1$  ( $p_x$ ) perpendicular wave from the  $s$  component of the DBS orbital as well as a  $d_{xz}$  wave from the  $p_z$  component of the DBS, the latter of which can be ignored when considering  $\beta$  as explained earlier.

In both cases, the electrons should have been ejected with at least some perpendicular amplitude (e.g., from the certainly large  $s$  orbital component of the DBS); however, in the experiment the angular distribution was found to be totally isotropic (see Figure 2 in ref 17) in both of these situations, which I now attempt to explain.

As explained earlier, in vibration-induced electron ejections, the KE is small, because it equals the vibrational energy (modes 11 and 18 have harmonic energies of 519 and 632  $cm^{-1}$ , respectively) minus the energy of the DBS relative to the neutral (97  $cm^{-1}$ ). For such small KEs, it is likely that only the wave having the lowest  $l_f$  value contributes, which would be the isotropic component when 538 nm photons were used and the  $p_x$  perpendicular component for 534 nm photons. The fact that

an isotropic rather than perpendicular distribution was found in the latter case suggests that the anion had time to rotate and lose its orientation memory before the nonadiabatic process had time to act. This suggests that the rate of the nonadiabatic electron ejection process was slow in comparison to the rate of molecular reorientation. Of course, it is also possible that KE is so small that  $Z^*(A^*KE) < 1$ , in which case  $\beta$  would be near 0.0 in both cases; however, this seems unlikely for two reasons: (i)  $Z$  is probably large, because the DBS orbital has substantially less  $p$  character than  $s$  character, and (ii)  $A$  is large (see eq 11), because the electron binding energy of this orbital is small.

When the laser's energy in ref 17 was not tuned to populate a selected vibrational mode of the DBS but was operated in the nonresonant mode discussed earlier, different angular distributions were observed. For example, when the photon energy was slightly above the ground vibrational level of the neutral but below any excited vibrational level of the DBS, only direct detachment of the  $b_1$  electron by an  $x$  ( $b_1$ ) symmetry photon to generate  $s$  and  $d_{x^2}$  waves can occur leaving the neutral in its ground vibrational state. At such photon energies, an isotropic angular distribution was observed (see the peak labeled  $0_0^0$  in Figure 1a in ref 17). This is consistent with the  $s$ -wave dominating at low KE. One would expect  $\beta$  to move to negative values at higher KEs as the  $d_{x^2}$  wave contributes and interferes with the  $s$ -wave to generate intensity perpendicular to  $x$  and as the  $d_{xz}$  polarization component of the  $b_1$  orbital interacts with the  $x$  photon to produce a  $p_z$ -wave. Indeed, at somewhat higher photon energies, the angular distribution seen in this nonresonant process changed (see peak  $0_0^0$  in Figure 1b of ref 15) and displayed significant perpendicular character arising from the interference between the  $s$  and  $d_{x^2}$  waves and perhaps from some  $p_z$ -wave electrons. In contrast, when mode 18 is populated in  $\nu = 1$  of the neutral (see peak  $18_0^1$  in Figure 1b) by a photon of  $z$  ( $a_1$ ) symmetry again in a nonresonant process, a parallel angular distribution is found. This happens because an  $a_1$  symmetry photon acting on the  $b_1$  orbital to generate a  $b_1$  vibration must eject electrons of  $a_1$  symmetry, which would be parallel to the photon's  $z$  polarization. Hopefully, this analysis offers another example of how angular distributions of ejected electrons depend on how the experiment is performed yet, when properly interpreted, offer much insight into the nature of the orbital from which the electron is ejected and the mechanism (i.e., direct electric dipole or nonadiabatic) by which the ejection occurs.

In 2020, a collaborative experiment<sup>19</sup> involving photodetachment from a nitro-benzene (NB) anion and electron capture by a neutral NB (via resonance states) produced results that also relate to the topic of this section. In the photodetachment component of that project, the workers observed direct detachment from the ground state of the  $NB^-$  anion into the ground state of the neutral NB including processes in which vibrational levels of the neutral were excited. They also found spectral peaks assigned to exciting the ground-state  $NB^-$  anion into a DBS of this anion. When the laser was tuned to populate infrared active vibrational modes of the DBS  $NB^-$  (i.e., modes that would modulate the DBS's loosely held electron), they detected low-KE electrons resulting from DBS-to-neutral and free electrons nonadiabatic  $\Delta\nu = -1$  transitions. Moreover, those workers were able to connect the intensities of peaks belonging to various vibrational modes to their calculated nonadiabatic coupling matrix elements of the corresponding electron-ejection processes.

Even more recently,<sup>20</sup> angular distribution data combined with vibrational mode-specific electron ejection findings were used to determine which isomer of the anion  $C_5N_2H_3O_2^-$  was formed when tetracyanoethylene (TCNE) anion reacts with methanol to produce the methyl-dicyanoacetate anion. The three anticipated structures of this product anion are shown in Figure 8a; they differ in terms of whether the two CN groups are attached to the same carbon atom and, if not, whether the two CN groups are cis or trans to one another.

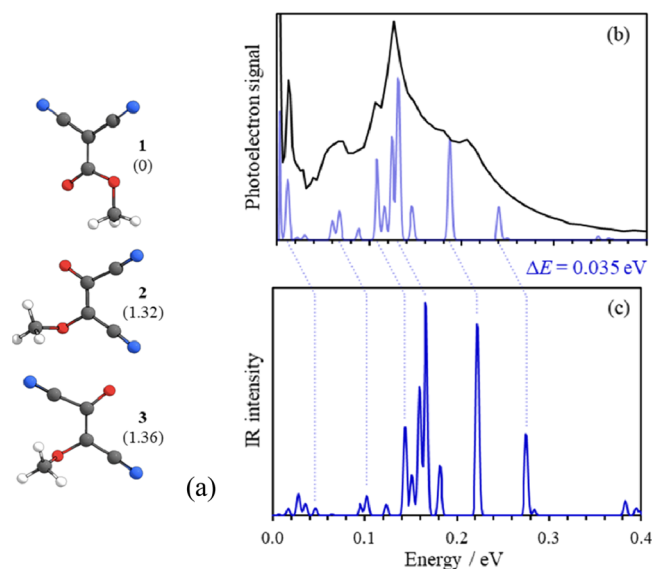


**Figure 8.** Three geometries of methyl-dicyanoacetate anion with their relative energies (eV) in parentheses (a). Photoelectron spectrum of isomer 1 using photons of 3.9 eV (black line in (b)) and computed IR spectrum (blue line in (c)) of this same isomer. (From ref 20).

The electronic structure calculations reported in ref 20 suggested that the isomer labeled 1 in Figure 8 is considerably more energetically stable (by 1.3–1.4 eV) than isomers 2 or 3, and the experimental findings confirmed this. It turned out that the angular distribution of electrons ejected with KEs between 0.1 and 0.6 eV by photons of 4.2 eV (the electron binding energy of isomer 1 is ca. 3.6–3.8 eV) was characterized by a negative  $\beta$  value, and the theoretically calculated  $\beta$  for isomer 1 was negative, while those for isomers 2 and 3 were positive. This

offers a good illustration of how angular distributions can be used to distinguish among geometrical isomers.

In addition, the workers of ref 20 showed how the computed IR spectrum of isomer 1 displayed an intensity versus energy profile (see the blue profile in Figure 8c, where the vibrations' energies are expressed in eV) that fits well<sup>21</sup> with the photoelectron intensity versus KE profile (see the black line in Figure 8b) of the species formed in the reaction of TCNE and methanol when the photon's energy is tuned to populate IR-active vibrations of the DBS of isomer 1. Of course, the fit requires that one subtract from the vibrational energies the electron binding energy of the DBS, which was 0.035 eV in this case. The IR spectra of isomers 2 and 3 did not produce such a match, which provided even more support to the claim that the anion formed in the reaction is isomer 1.

*III.B.2. Roll: Rotation as the Active Motion.* Thus far, I have discussed cases in which excess vibrational energy in the DBS can be converted into electronic energy to eject an electron, but it is also possible for excess rotational energy to play such a role. In the 1987 experiments of Lykke et al.,<sup>12</sup> the data shown in Figure 9 were obtained. The broad gradually rising signal arises from the direct photodetachment from various vibration/rotation levels of the  $^1A_1$  state of the anion (including from excited vibrational levels producing hot bands) to vibration/rotation levels of the  $^2B_1$  neutral. The sharper features arise from the resonance-enhanced process discussed earlier in which vibrational energy within the DBS ejects the electron via a nonadiabatic process.

When the experimental data were focused in a narrow range of photon energies near that of the peak designated by the arrow at the top of Figure 9, the authors of ref 12 discovered a pattern of peaks such as those shown in Figure 10. They were able to assign each of these peaks to a transition to a particular rotational level within a particular vibrational level of the DBA anion.

The  $H_2CCN^-$  anion is a near prolate asymmetric top, so its rotational energy levels can be labeled by  $J''$ ,  $K''$ , and  $M''$  quantum numbers with  $K''$  being the quantum number for rotation of the  $H_2C-$  group around the  $C_{2v}$  axis,  $J''$  labeling the total angular momentum, and  $M''$  labeling the component of the total angular momentum along a lab-fixed Z-axis.

It was observed in ref 12 that the line widths associated with the peaks shown in Figure 10 increased as the rotational quantum number  $J''$  increased but were not strongly dependent on the  $K''$  quantum number. At first, this might be surprising,

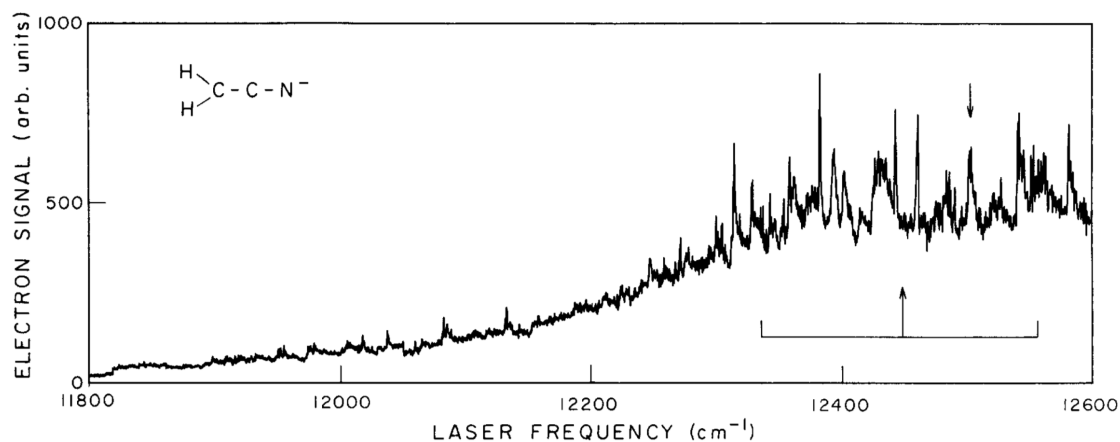


**Figure 9.** Plot of the intensity of electrons ejected from  $H_2CCN^-$  as a function of laser frequency ( $cm^{-1}$ ) (Reproduced from ref 12, with the permission of AIP Publishing).

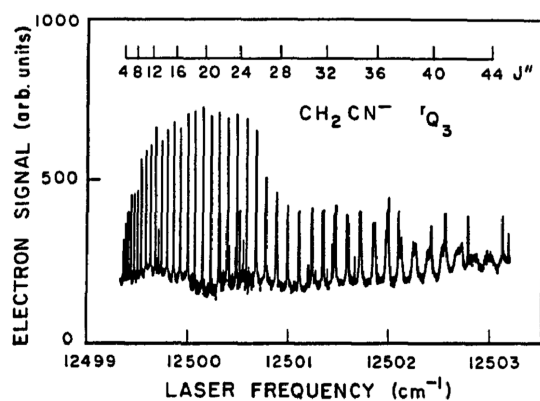


**Figure 10.** Plot of the intensity of electrons ejected as a function of laser frequency with the rotational quantum number ( $J''$ ) in the DBS of the anion labeled (Reproduced from ref 12, with the permission of AIP Publishing).

because the spinning of the  $\text{H}_2\text{C}-$  group about the  $C_{2v}$  axis contains a lot of rotational energy (because of the small moment of inertia associated with this degree of freedom, the energy spacings between neighboring levels can be large even for modest  $K''$ ). In fact, when the line widths (or converted into detachment rates) were plotted as a function of the total angular momentum quantum number for a fixed value of the  $K''$  quantum numbers, the plot shown in Figure 11 was obtained.<sup>12</sup>

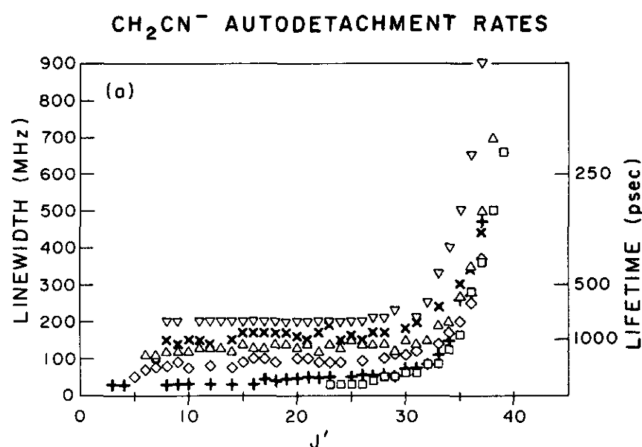


**Figure 11.** Plots of the observed line width for electron detachment from the DBS state of  $\text{H}_2\text{CCN}^-$  as a function of the total rotation quantum number for various values of the  $K''$  quantum number (labeled by the various symbols). (Reproduced from ref 12, with the permission of AIP Publishing).

The rate of rotation-induced electron ejection is seen to vary weakly with  $J''$ , until a critical value (ca.  $J'' = 30$ ) is reached, after which the rate increases rapidly. And even though rotations about the  $z$ -axis have larger energy gaps between their quantum states, this kind of motion has little influence on the dipole moment and hence on the  $a_1$  DBS orbital. The interpretation put forth by Lykke et al.<sup>12</sup> is that it is the tumbling rotation of the  $\text{H}_2\text{CCN}^-$  anion (i.e., rotations about the  $x$  or  $y$  axes in Figure 4) that induce the electron detachment, because it is this kind of motion that modulates the  $a_1$  DBS orbital holding the excess electron.

In 1988 Clary<sup>22</sup> put forth a quantum-based model (later modified slightly by this author<sup>23</sup>) in terms of which the energy flow from the rotations of the  $\text{H}_2\text{CCN}^-$  anion to the  $a_1$  DBS

electron can be quantitatively understood. As I will now illustrate, doing so is useful, because it uncovers selection rules involving a combination of angular momentum and energy conservation.

In the most basic version of this rotationally adiabatic model that would apply to a diatomic molecule<sup>24</sup> with a rotational constant  $b_v$  in vibrational state  $v$ , a Hamiltonian is introduced

$$H = b_v j^2 + V + \frac{l^2}{2m_e r^2} - \frac{\hbar^2}{2m_e r^2} \frac{\partial}{\partial r} \left[ r^2 \frac{\partial}{\partial r} \right] \quad (13)$$

and partitioned into two pieces

$$H^0 = b_v j^2 + V + \frac{l^2}{2m_e r^2} \quad (14)$$

the first describing the anion's rotation, the electron's angular kinetic energy, and the electron-molecule interaction, and the second being the electron's radial kinetic energy  $-\frac{\hbar^2}{2m_e r^2} \frac{\partial}{\partial r} \left[ r^2 \frac{\partial}{\partial r} \right]$ .

Here  $V$  is the electron-molecule interaction potential, which, in this model, is taken to be of the charge-dipole form

$$V(r, \theta) = -\frac{\mu}{r^2} F(r) \cos \theta \quad (15)$$

and the function  $F(r)$  serves to cut off the attractive potential as small  $r$ .

For each value  $J$  of the total (i.e., rotational and electronic) angular momentum of the electron-molecule system, various values of the rotational quantum number  $j$  and of the electron's angular momentum quantum number  $l$  are possible. These rotational  $|j, m\rangle$  and electronic  $|l, M - m\rangle$  angular momentum states can be coupled to form total angular momentum states

$$|J, M; j, l\rangle = \sum_m \langle j, m, l, M - m | J, M \rangle |j, m\rangle |l, M - m\rangle \quad (16)$$

where the  $\langle j, m, l, M - m | J, M \rangle$  are the well-known vector coupling coefficients.<sup>25</sup>

For given values of  $J$  and  $M$ , a set of rotationally diabatic energies (for all of the  $j$  and  $l$  values that can generate that total  $J$ ) are obtained

$$\begin{aligned} E_{j,l}^0(r) &= \langle J, M; j, l | H^0 | J, M; j, l \rangle \\ &= b_v j(j+1) \hbar^2 + \frac{l(l+1) \hbar^2}{2m_e r^2} \end{aligned} \quad (17)$$

The contributions from the potential  $V$  vanish because of the  $\cos(\theta)$  dependence of  $V$ . In Figure 12 I show several of these diabatic curves for the case  $J = 34$  with  $j, l$  varying from 34, 0 through 27, 7. Clearly the curve with  $l = 0$  is flat, while those having nonzero  $l$  display the  $r^{-2}$  character given in eq 17.

The parameters used to generate Figure 12 were chosen<sup>23</sup> to represent the  $a_1$  DBS of  $\text{H}_2\text{CCN}^-$  with the  $J = 0$  level of the neutral defining the energy origin, as a result of which the  $J = 0$  level of the anion has an energy of  $-60 \text{ cm}^{-1}$ , the  $J = 34$  ( $K = 0$ ) level of the anion has  $E = 346 \text{ cm}^{-1}$ , and the  $J = 34$  ( $K = 0$ ) level of the neutral has  $E = 406 \text{ cm}^{-1}$ . Given this set of diabatic energy surfaces, one then solves for lowest adiabatic surface, which is obtained by diagonalizing the matrix  $\langle J, M; j', l' | H^0 | J, M; j, l \rangle$  formed from the various  $j, l$  values. Because of the  $\cos(\theta)$  dependence of the potential  $V$ , only states differing by one unit of angular momentum contribute to the off-diagonal matrix elements (e.g.,  $j, l$  couples to  $j + 1, l - 1$  or to  $j - 1, l + 1$ ). This process generates a

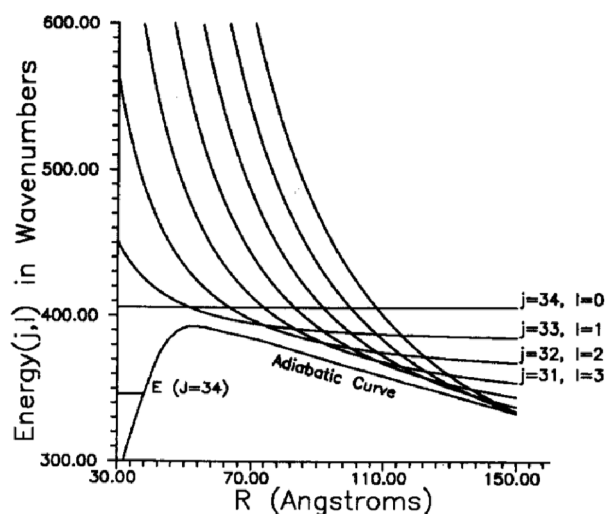


**Figure 12.** Rotationally diabatic energy surfaces appropriate to various  $j, l$  states of the DBS state of  $\text{H}_2\text{CCN}^-$  for a total  $J$  value of 34. Also shown are the lowest resultant adiabatic surface and the energy location of the DBS (Reproduced from ref 23, with the permission of AIP Publishing).

lowest adiabatic surface like that shown in Figure 12. Then using this adiabatic surface as the potential energy function in a Hamiltonian with the radial kinetic energy  $-\frac{\hbar^2}{2m_e r^2} \frac{\partial}{\partial r} \left[ r^2 \frac{\partial}{\partial r} \right]$  in place, one can calculate the rate of tunneling through the barrier on this surface. It is this rate that Clary showed<sup>22</sup> models the rotation-induced nonadiabatic electron ejection observed in ref 12.

Three observations about the rotation-induced ejection process are important to make. First, it is those rotational motions that couple strongly (i.e., modulate in space) to the DBS orbital that are most important even if these motions do not have the highest energy content. Second, the rate of electron ejection increases with the rotational quantum number<sup>26</sup>  $J$ . Third, for a given rotational quantum number  $J$  of the DBS anion, the quanta of angular momentum transmitted to the electron  $l$  can differ from  $J$  by various values (i.e.,  $\Delta l$  need not be small).

Let us illustrate this final point, because it is especially important to appreciate. By following the diabatic energy curves in Figure 12 out to  $r \rightarrow \infty$ , one can see that the  $J = 34$  state of the DBS anion (which corresponds at small  $r$  to the molecule in  $j = 34$  and the DBS electron in  $l = 0$ ) lies barely above the  $j = 31, l = 3$  state of the neutral. It is energetically impossible for this  $J = 34$  state to decay into  $j = 32, l = 2$  or  $j = 33, l = 1$ . So, for this system in  $J = 34$ , only transitions involving three or more quanta of rotations ( $\Delta J \leq -3$ ) are energetically “allowed”. This, in turn, means that the ejected electrons must have  $l \geq 3$  (i.e., they can detach with angular distributions having  $l = 3, 4, 5, \dots, 34$  components).

Such energy constraints as well as the angular momentum selection rules embodied in the above model are what govern this kind of process. It is relatively easy to see how this energy constraint condition arises. Knowing that the DBS lies ca.  $\Delta E = 60 \text{ cm}^{-1}$  below the neutral’s ground state and assuming that the rotational constant  $b_v$  is the same for the DBS anion and the neutral (because they have very similar geometries), one can determine the highest  $j_f$  level of the neutral that is energetically accessible from a given initial  $j_i$  level of the DBS using

$$-\Delta E + b_v j_i(j_i + 1) \geq b_v j_f(j_f + 1) \quad (18)$$

which gives the following condition on the change in  $j$ -values  $j_f - j_i = -\Delta j$

$$[2j_i + 1 - \Delta j] \geq \frac{\Delta E}{\Delta j b_v} \quad (19)$$

For any given  $j_i$ , the transition leaving the neutral molecule in the highest value of  $j_f$  that obeys eq 18 will eject electrons with the lowest KEs (i.e., the KE is determined by the amount by which the left side of eq 18 exceeds the right side). Transitions into lower values of  $j_f$  will eject electrons with higher kinetic energies (e.g., having

$$\text{KE} = \text{KE}_{j_f}^0 + b_v [j_f^0(j_f^0 + 1) - j_f(j_f + 1)] \quad (20)$$

where  $j_f^0$  is the highest value of  $j_f$  obeying eq 18.

Applied to the case at hand for which  $\Delta E = 60 \text{ cm}^{-1}$  and  $b_v = 0.3 \text{ cm}^{-1}$ , this equation shows that, for a  $\Delta j = 1$  transition,  $j_i$  must exceed 100, for a  $\Delta j = 2$  transition,  $j_i$  must exceed 50, for a  $\Delta j = 3$  transition,  $j_i$  must exceed 35, and for a  $\Delta j = 4$  transition,  $j_i$  must exceed 27. Of course, the initial rotational quantum number  $j_i$  must be large enough to make  $-\Delta E + b_v j_i(j_i + 1) > 0$ , which for the case at hand requires  $j_i > 13$ . In this limiting case, the final quantum number  $j_f$  would have to be zero, so  $\Delta j$  would be 13. As can be seen from Figure 12, the larger  $\Delta j$  is, the higher and wider will be the centrifugal barrier through which the electron must tunnel. This is why the electron ejection rates increase greatly with the rotational quantum number of the anion once a critical value is reached; below that critical value,  $\Delta j$  is large, and the barrier is high and wide.

Before leaving this example, it is worth reminding the reader that the rotation-induced electron ejection can be expected to produce free electrons in quite high angular momentum states and with a wide range of KEs. For the example illustrated in Figure 12, the  $J = 34$  state of the DBS anion would eject electrons having  $l \geq 3$ , because this anion state lies just above the  $j = 31, l = 3$  diabatic energy level but below all anion states with  $j > 31$  and  $l < 3$ . The electrons ejected in the  $l = 3$  wave would have low KE; those ejected in  $l = 4$  and higher- $l$  waves would have higher KEs as explained above (see eq 18). This suggests that angular distribution data could be of use in probing these processes if control over the orientation of the  $J$  vector of the DBS could be realized. It also suggests that KE data for the ejected electrons could be of use if sufficient energy resolution exists to exploit it.

**III.C. Shine–Shine: Two-Photon Probing of the  $^1\text{B}_1$  Dipole-Bound Anion.** One photon whose energy is tuned to the  $\nu = 0$  level of the  $^1\text{B}_1$  DBS anion could be used to excite the anion from its  $^1\text{A}_1$  ground state into this lowest vibrational level of the DBS. Again assuming the anion to be aligned as in Figure 4, this requires a photon of  $x(b_1)$  polarization to generate the  $\nu = 0$   $^1\text{B}_1$  DBS. A second photon can then be used to detach an electron from the  $a_1$  symmetry DBS orbital, and the angular distribution of these electrons can be measured as suggested in Figure 13. Note that the treatment that follows could be applied to the study of anions whose ground state is a DBS (i.e., in this case, one can ignore the first photon that created the DBS).

Once the DBS is formed, there are two distinct phenomena that can take place. The second photon, which need not be resonant with any particular transition, can induce a direct electric dipole detachment from the DBS’  $\nu = 0$  level into various vibrational levels of the  $^2\text{B}_1$  neutral generating a free electron. This is another example of a nonresonant electron detachment

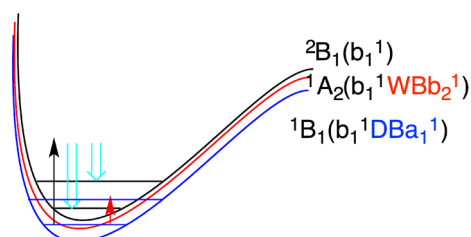


**Figure 13.** Depiction of photodetachment by a second photon (black arrow) from the  ${}^1B_1(b_1^1DBa_1^1)$  excited anion into the  $\nu = 0$  and  $\nu = 1$  levels of the neutral with the kinetic energies of the ejected electrons illustrated by aqua arrows. The red arrow applies when the second photon resonantly excites a vibrational level of the BDS anion (in this case from  $\nu = 0$  to  $\nu = 1$ ).

process. Another thing can happen if the second photon is tuned to allow it to resonantly vibrationally excite the DBS as suggested by the red arrow in Figure 13. In this case, the second photon actually can do two things: (i) vibrationally excite the DBS (e.g., into  $\nu = 1$  of some mode) after which a vibration-to-electronic shake/rattle nonadiabatic transition can occur to eject an electron leaving the  ${}^2B_1$  neutral in its  $\nu = 0$  level, or (ii) directly detach an electron from the DBS again leaving the  ${}^2B_1$  neutral in  $\nu = 0$ . It is in such cases that the issue of Fano line shapes arises, and I will discuss this situation immediately after treating the nonresonant situation mentioned above—the direct detachment from  $\nu = 0$  in the DBS into various vibrational levels of the neutral.

**III.C.1. The Direct Detachment Pathway and Its Angular Distribution.** If the  ${}^1B_1(b_1^1DBa_1^1)$  anion formed in the initial photon absorption event does not have time to reorient prior to the absorption of a second photon, the angular distribution of the ejected electrons can be related to the polarization ( $x$ ) of the first photon as well as to that of the second photon, which may or may not be the same as for the first photon. In particular, again referring to Table 1, assuming the anion is oriented along the  $z$ -axis and that any vibration excited in the ejection process has  $a_1$  symmetry (so I do not have to consider the vibration's symmetry contribution)

- a second photon of  $z$  ( $a_1$ ) polarization will eject electrons of  $a_1$  symmetry with the  $p_z$  wave arising from the  $s$  component of the DBS being parallel to the second photon. From the  $p_z$  component of the DBS there will also be  $s$  and  $d_{z^2}$  waves producing isotropic and parallel emission (relative to the second photon) as well as interference perpendicular to the second photon; however, the  $p_z$  wave should dominate, because the DBS orbital likely has little  $p$  character.
- a second photon of  $x$  ( $b_1$ ) polarization when acting on the  $s$  component of the DBS will eject electrons of  $b_1$  ( $p_x$ ) symmetry<sup>27</sup> and thus be parallel to the second photon.
- a second photon of  $y$  ( $b_2$ ) polarization acting on the  $s$  component of the DBS will eject electrons of  $b_2$  ( $p_y$ ) symmetry parallel to the  $y$ -polarization of the second photon.

Of course, if the  ${}^1B_1(b_1^1DBa_1^1)$  anion formed in the initial photon absorption event had ample time to reorient prior to the absorption of the second photon, the information relating the ejected electrons' spatial distribution would only be retained with respect to the polarization of the second photon.

**III.C.2. The Resonance-Enhanced Pathway and the Origin of Fano Lineshapes.** If the second photon is tuned to

vibrationally excite the DBS to, for example,  $\nu = 1$  in some mode at which the  $\nu = 0$  energy (in the same mode) of the neutral is lower in energy, then a  $\Delta\nu = -1$  nonadiabatic transition [ ${}^1B_1(\text{DBS}); \nu = 1$ ]  $\rightarrow$  [ ${}^2B_1 + e^-; \nu = 0$ ] can take place. The propensity for such  $\Delta\nu = \pm 1$  transitions was explained in 1981.<sup>16</sup>

This same second photon can alternatively simply access the [ ${}^2B_1 + e^-; \nu = 0$ ] final state via a direct detachment from the [ ${}^1B_1(\text{DBS}); \nu = 0$ ] state. Especially in cases where the direct ejection and vibrational excitation followed by nonadiabatic ejection events involve a DBS, these two competing processes combine in a manner that can lead to an unusual line shape for the yield of ejected electrons as a function of photon energy. Why especially in this case? Because both the transition dipole matrix element for the (infrared) vibrational excitation process and the nonadiabatic coupling matrix element for the vibration-to-electronic energy flow process depend linearly on the derivative of the dipole moment with respect to the excited vibrational mode's coordinate  $\frac{d\mu}{dQ}$  (see the Supporting Information for more details). For this reason, the final-state wave function is a superposition of two terms that can be of similar magnitude—one relating to the direct detachment mechanism and the other relating to vibrational excitation followed by nonadiabatic energy flow.

In 2012, Edwards et al.<sup>28</sup> showed how this kind of two-channel phase-dependent process can give rise to the so-called Fano lineshapes for infrared-induced electron ejection in DBS of  $(\text{H}_2\text{O})_n^-$  anions. In Figure 14 I show data from Hammer et al.<sup>29</sup>

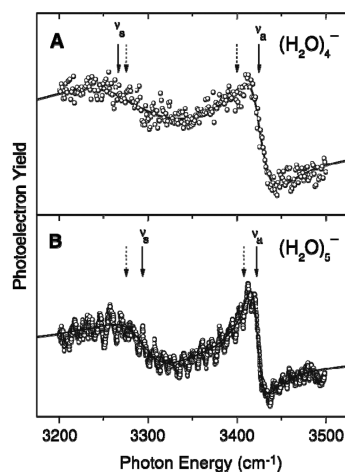


**Figure 14.** Plot of electron ejection yield as a function of photon energy for two different water cluster anions that bind the excess electron in a DBS manner. The labels  $\nu_s$  and  $\nu_a$  denote the frequencies of the symmetric and asymmetric O–H stretches of the clusters' water molecule closest to the DBS electron (From ref 29. Reprinted with permission from AAAS).

on such anions in which the electron loss yield is plotted as a function of the energy of the photons used to effect the detachment. The interference between the two processes gives rise to the oscillation of the electron yield, above and below the direct-detachment baseline, shown in Figure 14.

**III.C.3. An Example of How Electron Ejection from Very Diffuse Orbitals Can Display Unusual Angular-Distribution Behavior.** Earlier, I explained how an orbital having a very small electron binding energy could produce an  $A$  factor (see eqs 10 and (11)) that is large and that then gives rise to unexpected

behavior in how the angular distribution's  $\beta$  parameter varies with KE. In this section I provide an example of how this happens.

In 2018, Rogers et al.<sup>30</sup> used pump–probe methods to follow the time evolution of a weakly bound state of  $C_6F_6^-$  formed when the pump laser ejected an electron from an  $I^- \cdots C_6F_6$  complex, and the electron was captured by the  $C_6F_6$  molecule. In 2014, Voora et al.<sup>31</sup> performed theoretical calculations on the  $C_6F_6^-$  anion focusing on its planar correlation-bound state (CBS) and on how this state evolves into a more strongly valence-bound state (VBS) when the  $C_6F_6$  unit undergoes a ring-buckling distortion.

In Figure 15 I show a depiction of how the experiments of ref 30 work. One sees at the bottom left a picture of the  $I^-$  5p orbital,

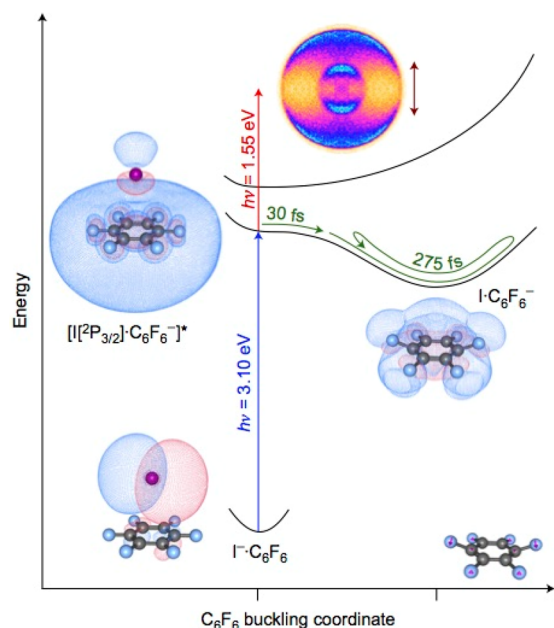


**Figure 15.** Depiction of photoinduced electron ejection from  $I^-$  onto  $C_6F_6$  by the first laser (3.10 eV) accessing the CBS of  $C_6F_6^-$  followed, after a time-variable time delay, by a second laser (1.55 eV) that ejects electrons from the  $C_6F_6^-$  (Reprinted by permission from Springer Nature: ref 30).

from which the electron is ejected by the first laser, and above that I show a picture of the orbital localized mainly on the  $C_6F_6^-$  belonging to the CBS. This state of the anion lies ca. 0.4 eV below the energy of the neutral  $C_6F_6$  at the geometry accessed by the pump laser, so the 1.55 eV probe laser detaches electrons with KE values near 1.1 eV if this probe laser is fired with a very short delay time (so the geometry does not have time to change much). Moreover, because the geometry of the weakly bound  $C_6F_6^-$  is very similar to that of the neutral  $C_6F_6$ , these photoelectrons are ejected over a narrow range of KEs.

In ref 30 it was observed that the intensity of electrons ejected by the probe laser with KEs near 1.1 eV decreased in less than 40 fs (i.e., the time between the pump and probe photons' arrival) and that the KE distribution of the electrons shifted to lower values over ca. 100 fs. This was interpreted to mean, as suggested in Figure 14, that, after its initial formation in a near-planar geometry, the  $C_6F_6^-$  anion undergoes a geometrical distortion that lowers its electronic energy and increases the energy gap between the anion and the neutral molecule. Voora et al. had shown<sup>31</sup> that buckling of the C–F bonds in the  $C_6F_6$  ring as

shown in Figure 16 is likely the deformation that leads from the CBS formed by the first laser into a more strongly bound VBS

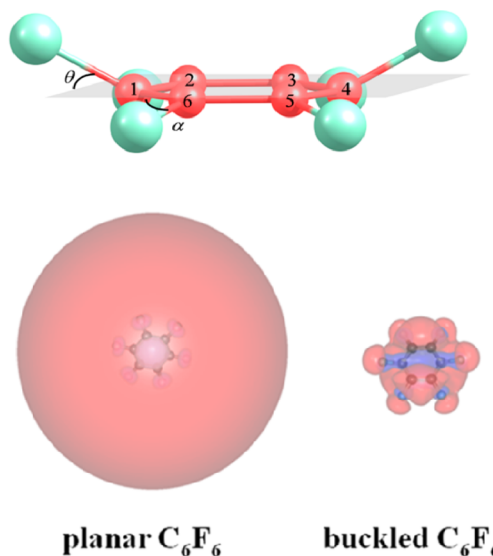


**Figure 16.** Proposed buckling of the  $C_6F_6$  C–F bonds to distort the anion (top) together with the orbitals occupied by the excess electron in  $C_6F_6^-$  in the planar and buckled geometries, respectively (bottom). (Adapted with permission from ref 31. American Chemical Society).

probed by the second laser at longer times. It was suggested that the VBS lies vertically ca. 1.45 eV below the neutral at its minimum-energy geometry, so its detachment by the probe laser generates electrons with lower KEs (e.g., over a range from 1.0 to 0.1 eV as the molecular framework moves from a planar to a buckled geometry).

One interesting feature that arose in the experiments of ref 30 was the observation of oscillation of the  $C_6F_6^-$  back and forth between the valence-bound state and the correlation-bound state. The intensity of electrons ejected at low KE (from the VBS) was found to oscillate in time with a period of ca. 275 fs, which is close to that expected for the ring-buckling vibrational mode of the  $C_6F_6^-$  anion.

The findings in the experiments of ref 30 on  $C_6F_6^-$  also displayed some unexpected but informative data related to the angular distribution of the electrons ejected by the probe photon, and it is to these findings that I now turn our attention. Specifically, the values of the  $\beta$  parameter found to fit the electrons ejected with KEs near 1.1 eV (i.e., from the CBS) turned out to be  $\beta = \text{ca. } 1.0$ , while  $\beta$  for the VBS was found to be  $\beta = \text{ca. } 2.0$  as shown in Figure 2b of ref 30. On the one hand, these  $\beta$  values are unexpected, because, for an orbital as spherically symmetrical as that shown in Figure 15 for the CBS, one would expect electron photoejection from an orbital of s symmetry and to thus find ejected electrons in a p-wave (parallel to the photon polarization), as a result of which  $\beta$  should be close to 2.0, not 1.0 as observed. On the other hand, the orbital of the VBS appears to be symmetrical but less so than the orbital of the CBS. Nevertheless, its  $\beta = 2.0$  is in line with ejection from an orbital of s-symmetry to produce p-wave electrons.

To understand how these  $\beta$ -value findings might be explained, I refer back to eq 8, where  $\beta$  is expressed in terms of the electron kinetic energy, the  $A$  parameter that contains information about the ratio of the  $p \rightarrow d$  and  $p \rightarrow s$  detachment cross sections, and the  $Z$  parameter that depends on the ratio  $(1-f)/f$  of the s-to-p orbital amplitudes in the orbital from which the electron is

ejected. I also refer back to our earlier discussion about how a very diffuse orbital can give rise to a large  $A$  factor (see eq 11 and the discussion following it), from which it is clear that an orbital having a very small electron binding energy (BE) will have a large  $A$  factor. So, I suggest that the  $\beta$ -value findings discussed above can be rationalized as follows:

- For both the CBS and the VBS, it appears that the amplitude of s-orbital character (see Figure 15) is larger than that of p-orbital character; so, the ratio  $(1-f)/f$  will be greater than 1. Also, given what is shown in ref 11 about the ratio  $B/A$  (that it is in the range from  $8/3$  to  $5/3$ ), this means that the  $Z$  parameter (see eq 9) will be greater than 1.
- The orbital of the CBS appears to be closer to s-symmetry than does the orbital of the VBS, so the ratio  $(1-f)/f$  for the CBS (and hence  $Z$ ) is likely larger for the CBS than for the VBS.
- Because the BE value of the CBS (0.4 eV) is less than that of the VBS (1.45 eV), the  $A$  parameter of the CBS will be larger than for the VBS, as eq 11 suggests.
- The key assumption that I now make is that, for the CBS, the factor  $A^*KE$  is larger than  $Z$  over much of the range of values of KE being probed, while for the VBS, the factor  $A^*KE$  is smaller than  $Z$ . The basis for making this assumption will be explained briefly, but, for now, I illustrate how this leads to rationalization of the  $\beta$ -value findings.
- For the CBS, assuming that  $A^*KE > Z$  (and realizing that  $Z > 1.0$ ) allows the expression for  $\beta$  in eq 8 to be reduced to  $\beta = \frac{2(A^*KE)^2}{2(A^*KE)^2} = 1.0$  at high KE.
- For the VBS, assuming that  $A^*KE < Z$  (but with  $Z$  still  $> 1$ ) allows the expression in eq 8 to be reduced to  $\beta = \frac{2Z^*(A^*KE)}{Z^*(A^*KE)} = 2.0$  at high KE.

These results are in line with the experimental findings in ref 30, where the authors also say that their ab initio calculations give these same  $\beta$ -values, which suggests that the ab initio methods accurately estimate the ratio of the  $p \rightarrow d$  to  $p \rightarrow s$  cross sections.

Now, I am faced with explaining why it makes sense to assume  $A^*KE > Z$  for the CBS and  $A^*KE < Z$  for the VBS. There are two factors contributing to making these assumptions likely valid. First, for the CBS, the electrons are ejected with higher KEs than for the VBS as explained earlier. Another factor is that the  $A$  parameter for the CBS is likely considerably larger than for the VBS, and it is this issue to which I now turn our attention, because it is the large  $A$  factor that plays a key role in our rationalization of the data.

As discussed earlier, in ref 11 it was shown that the  $A$  parameter could be related to the orbital exponent  $\xi$  characterizing the asymptotic behavior of the p-orbital component of the active orbital (recall that  $A$  described the ratio of  $p \rightarrow d$  and  $p \rightarrow s$  detachment cross sections). Certainly, the CBS is less strongly bound and thus more diffuse, so its  $\xi$  will be smaller than for the VBS (see eq 10), and thus its  $A$  will be larger. However, I suggest that the dependence of  $A$  on the orbital's BE given in eq 10 or equivalently in eq 11 is not the only factor operative for anions like  $C_6F_6^-$ .

The derivation of eq 10 presented in ref 11 assumes that the active orbital is of 2p radial character (recall that  $A$  relates to the  $p \rightarrow d$  and  $p \rightarrow s$  cross sections) and that the origin of the coordinate system within which both this active orbital and the

s- and d-wave ejected electrons' orbitals are expressed sits where this 2p orbital has its origin. However, I wish to offer an alternative description that I believe is more appropriate for the kind of anion discussed here. In particular, I view the coordinate origin being at the center of the planar  $C_6F_6^-$  anion but with most of the orbital's density involving a combination of atomic orbitals whose centers reside on a spherical shell of radius  $R$  (e.g., see Figure 16) where the carbon and fluorine atoms are located. To characterize such an orbital, especially where its amplitude is largest and outward into its asymptotic region, I propose using the following expression

$$R_{WBS}(r) = Nr^\alpha \exp(-\gamma r) \quad (21)$$

where  $N$  is a normalization constant, WBS refers to weakly bound state CBS or VBS in this example, and the parameter  $\alpha$  is chosen so that the maximum in this orbital occurs at the presumed spherical shell  $r = R$ , which gives  $\alpha/\gamma = R$ . The exponential parameter  $\gamma$  is expressed in terms of the electron binding energy (in atomic units) as

$$\gamma = \sqrt{2BE} \quad (22)$$

in order to provide the correct asymptotic behavior,<sup>32</sup> so this means that  $\alpha = R\gamma = R\sqrt{2BE}$ . Taking  $R_{WBS}(r)$  to be of this form and evaluating the two radial integrals needed to determine the  $A$  parameter (see eq 21 of ref 11) gives

$$\begin{aligned} A &= \frac{2 \int_0^\infty r^5 R_{WBS}(r) dr}{15 \int_0^\infty r^3 R_{WBS}(r) dr} \\ &= \frac{2 (5 + R\sqrt{2BE})(4 + R\sqrt{2BE})}{15 \cdot 2^*BE} \text{Ha}^{-1} \\ &= \frac{1 (5 + 0.27R\sqrt{BE})(4 + 0.27R\sqrt{BE})}{15 \cdot BE} \text{eV}^{-1} \end{aligned} \quad (23)$$

In the final expression,  $R$  must be expressed in angstroms, and BE is in electronvolts. Clearly, this model for the  $A$  parameter can produce larger values than those based on eq 11 for species whose active orbital's radial extent is spread over a large region as characterized by  $R$ . Notice that this expression is similar to that in eq 11 in that both suggest  $A$  grows approximately as  $1/BE$ . Equations 23 and (11) differ in their numerators, where eq 11 has a product  $(n+4) \times (n+3) = (5+1) \times (4+1)$  for a 2p orbital, while eq 23 contains the product  $(5 + 0.27R\sqrt{BE})(4 + 0.27R\sqrt{BE})$ , and the factor  $0.27R\sqrt{BE}$  can exceed 1.0 when  $R$  is large.

When applied to the CBS and VBS of  $C_6F_6^-$  (in ref 30 the estimate  $R = 10 \text{ \AA}$  is given for the CBS, and I estimate  $R = 5 \text{ \AA}$  for the VBS; and I take BE = 0.4 and 1.45 eV, respectively, from ref 30), eq 23 yields  $A = 6.4 \text{ eV}^{-1}$  for the CBS and  $1.8 \text{ eV}^{-1}$  for the VBS. Both of these  $A$  values exceed by a small amount what eq 11 produces (5.0 and  $1.4 \text{ eV}^{-1}$ , respectively). Note that both  $A$  factors are larger than those cited earlier for  $H_2N^-$  and  $Cl_2C^-$  (0.37 and  $0.75 \text{ eV}^{-1}$ , respectively), where detachment occurred from a nitrogen or carbon 2p or 2s orbital. It is worth reminding the reader that, for electrons in dipole-bound orbitals, where BE can be very small, (e.g.,  $100 \text{ cm}^{-1} = 1.2 \times 10^{-2} \text{ eV}$ ),  $A$  can be even larger than what I find for  $C_6F_6^-$ . For example, for BE =  $100 \text{ cm}^{-1}$ , eq 11 predicts  $A = \text{ca. } 160 \text{ eV}^{-1}$ . This suggests that somewhat unusual KE dependences of  $\beta$  can arise in DBS species, as they do in the  $C_6F_6^-$  case discussed here. However, the fraction  $f$  of p-orbital character in a DBS orbital might be so

small as to make the  $Z$  parameter so large that the  $A^*KE > Z$  condition is not satisfied for accessible KE values.

Finally, let us return to how a large  $A$  can produce the unusual  $\beta$  values found in ref 30. Because electrons are ejected with KE in the 1.1 eV range for the CBS, the factor  $A^*KE$  will be ca. 7 for this state. In contrast, for the VBS, the electrons have KEs near 0.1 eV, so  $A^*KE$  will be ca. 0.2. Assuming that  $B/A = 8/3$  (as explained earlier for a state based on 2s and 2p orbitals) and using  $Z = \frac{B^{1-f}}{A^f}$ , I can conclude that, for  $Z < 7$  (the  $A^*KE$  value) for the CBS to be true,  $f > 8/29$  must hold, and for  $Z > 0.2$  for the VBS to be true,  $f < 8/8.6$  must hold. It is worth mentioning that, if 0.14 eV were assumed for the electron binding energy of the CBS (an alternative mentioned in ref 30), an  $A$  value of  $14 \text{ eV}^{-1}$  would result, and for  $Z < 14 \text{ eV}^{-1} \times 1.1 \text{ eV} = 15$  to be valid,  $f > 8/53$  must hold. The constraint on  $f$  for the VBS is nearly certain to be true, and for the CBS it is quite possible. It is on this basis that I offer the rationalization that  $A^*KE > Z$  for the CBS, while  $A^*KE < Z$  for the VBS, which then produces  $\beta = 1.0$  for the former and  $\beta = 2.0$  for the latter. It would be informative if the data on the CBS could be re-examined to determine what  $A$  value could fit the  $\beta(\text{KE})$  versus KE profile that leads to  $\beta = 1.0$  at high KE. If that  $A$  were  $6.4 \text{ eV}^{-1}$  or larger, that would offer further support for our rationalization.

In the Supporting Information, I give an alternative model of estimating  $A$  based on modeling the active orbital in terms of 2p orbitals localized a distance  $R$  from the origin. That model gives very similar estimates to the  $A$  values reported above. I do not mean to suggest that eq 23, eq 11, or what is in the Supporting Information provides a highly accurate value for the  $A$  parameter; certainly extracting  $A$  from experimental  $\beta(\text{KE})$  data or using ab initio methods offers more accurate paths. Our analytical expressions are meant to offer understandable explanations of how large  $A$  values can arise for species with small BE values and/or when the excess charge is spread over a large radius  $R$ .

**III.D. Shine and Roll: Rotational-to-Electronic Energy Flow to Populate a Hypothetical Higher-Lying but Optically Dark  $^1A_2$  WBS of the Anion.** If there really were a WBS anion state that was optically dark relative to the  $^1A_1$  anion's ground state but lying above the  $^1B_1$  DBS discussed earlier, it might be accessed by nonadiabatic transitions from the  $^1B_1$  DBS as suggested in Figure 17.

Assuming that the DBS and the WBS both lie very close in energy to the  $^2B_1$  neutral (e.g., the DBS of  $\text{H}_2\text{CCN}^-$  lies only ca.  $60 \text{ cm}^{-1}$  below the neutral), it is likely that the separation in the electronic energies of these two states is quite small. This means that the vibration/rotation-to-electronic nonadiabatic transition that might be operative requires little energy to be given to the

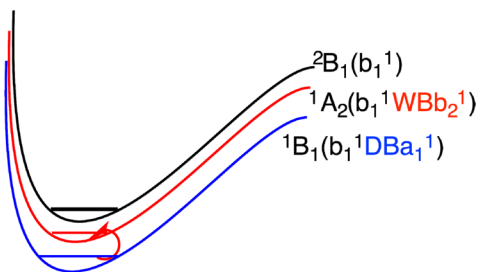


**Figure 17.** Depiction of the nonadiabatic process in which the rotation energy of the DBS is used to induce the  $a_1$ -to- $b_2$  electronic orbital excitation to generate the WBS.

electronic degree of freedom to effect detachment. For this reason, it would be more likely<sup>33</sup> for the transition to involve energy transfer from a rotational motion of the molecular framework than from a vibration, and it is this possibility that I now consider.

Given that the WBS lies  $\Delta E' < 60 \text{ cm}^{-1}$  above the DBS, this is the amount of rotational energy the DBS would have to contribute to the transition. Since the DBS orbital is of  $a_1$  symmetry and, by assumption in our example, the WBS orbital is of  $b_2$  symmetry, the rotational motion has to be of  $b_2$  symmetry. This symmetry selection rule arises because the nonadiabatic transition matrix elements  $\langle \Psi_f | \nabla | \Psi_i \rangle \bullet \langle \Phi_f | \nabla | \Phi_i \rangle$  involve the dot product of (i) an integral between the initial ( $a_1$ ) and final ( $b_2$ ) orbitals ( $\Psi_{i,f}$ ) in which only the  $b_2$  component of the vector operator  $\nabla$  contributes with (ii) an integral  $\langle \Phi_f | \nabla | \Phi_i \rangle$  over the initial and final rotational wave functions ( $\Phi_{i,f}$ ) in which only the same  $b_2$  component of  $\nabla$  appears. This means that the rotation would have to involve motion about the  $x$ -axis of the  $\text{H}_2\text{CCN}^-$  anion (see Figure 4). Spinning of the  $\text{H}_2\text{C}$  group about the  $z$ -axis is of  $a_1$  symmetry and would not be operative in the nonadiabatic energy transfer nor would rotation about the  $y$ -axis, because that rotation is of  $b_1$  symmetry.

When it comes to which rotational levels would be involved, and realizing as was just pointed out that  $z$ -axis motion is inoperative, the simple model used earlier in Section III.B.2 can offer insight. Assuming that the tumbling rotation of the anion can be approximately described in terms of a rigid-rotor, its  $j, m$  energy levels are given by

$$E_{j,m} = b_v j(j+1) \quad (24)$$

where  $b_v$  is the rotational constant (for rotation about the  $x$ -axis) of the  $\nu$ th vibrational level. The rotational matrix element  $\langle \Phi_f | \nabla | \Phi_i \rangle$  entering into the nonadiabatic coupling can only connect states whose  $j$ -values differ by one unit of angular momentum. The energy  $\Delta E'$  required to effect the orbital change must match a  $j \rightarrow j-1$  rotational transition, whose energy spacing is given by  $2(j+1)b_v$ . This means the rotational states that will be depopulated by nonadiabatic conversion of  $\Delta E'$  of rotational energy into  $^1B_1$ -to- $^1A_2$  electronic energy should have

$$j+1 = \frac{\Delta E'}{2b_v} \quad (25)$$

Applied to the  $\text{H}_2\text{CCN}^-$  anion (whose  $b_v = 0.3 \text{ cm}^{-1}$ ) and assuming that ca.  $30 \text{ cm}^{-1}$  of energy separates the DBS and WBS (i.e., placing the WBS half way between the DBS and the neutral), this suggests that rotational states near  $j = 49$  would be involved.

Notice that this selection rule is very different from the constraint eq 18 that applies to the rotation-induced electron ejection. In the present case, the fact that the orbital transition is constrained to be of  $a_1$ -to- $b_2$  symmetry with the  $a_1$  orbital having mainly  $l = 0$  character and the  $b_2$  orbital having primarily  $l = 1$  character means that the orbital  $l$ -value changes by one unit in angular momentum. This is why the rotational de-excitation involves  $j \rightarrow j-1$ . In the electron ejection case, the final  $l$ -value of the ejected electron is not constrained; it can be any value that obeys eq 18 for a given  $j_i$  value.

To probe for this kind of nonadiabatic process using electron detachment, one could, after using one photon to populate the DBS, perform photodetachment from this state and look for indications that another state (e.g., the WBS) has been

populated. On the one hand, for the  $\text{H}_2\text{CCN}^-$  anion being used as an example, detachment of an electron from the  $a_1$  orbital (having mainly  $s$  and little  $p$  character) of the DBS would be expected to eject electrons (i) with KE equal to the photon energy minus the binding energy of the DBS (ca.  $60\text{ cm}^{-1}$ ) and (ii) with an angular distribution consisting of primarily parallel components (see Table 1) because of the dominance of the  $s$ -orbital character in the DBS. On the other hand, if the  $b_2$  orbital (directed along the  $y$ -axis in Figure 4) in the WBS were populated by the nonadiabatic process, subsequent photon-induced detachment of an electron from it would eject electrons (i) with KE (slightly) greater than for the DBS and (ii) with an angular distribution consisting of isotropic and perpendicular components (see Table 1) arising from the  $s$ - and  $d_{y^2}$ -waves and their interference. In addition, if rotational resolution were accessible, one could look for a depletion of rotational levels that effected the nonadiabatic transition (i.e., those obeying eq 25 for our example).

At the time this manuscript was initiated, I was unaware of any molecular anion that has yet been shown to possess a DBS and another WBS at the same geometry (i.e., very near that of the neutral). The Bowen group<sup>34</sup> had shown that 1,4-dicyanocyclohexane in its *cis* isomer (having a dipole moment of 5.9 D) has a DBS, while this same molecule in its *ee-trans* isomer has a quadrupole-bound state. This situation had earlier been predicted by Sommerfeld et al.,<sup>35</sup> but this does not offer an example directly related to the case I treated above, because the two weakly bound states do not exist at the same geometry.

However, upon nearly completing this manuscript, I became aware of a case that does purport to display two weakly bound states connected by a nonadiabatic transition much like I just discussed.<sup>36</sup> In that work, an optically dark weakly bound state was suggested to lie below the DBS state of  $a_1$  symmetry that was populated by photon absorption from the valence-bound ground state of the  $\text{C}_{14}\text{H}_9\text{O}^-$  anion formed by deprotonating 9-anthrol. This molecule has a large dipole moment (3.6 D) directed along its  $C_{2v}$  symmetry axis, and its delocalized  $\pi$ -electron rings produce a very large polarizability perpendicular to the  $C_{2v}$  axis. The authors of ref 36 suggest that the large dipole moment gives rise to the  $a_1$  symmetry DBS, while a combination of the large dipole moment and the large polarizability give rise to a second weakly bound state of  $b_2$  symmetry as illustrated in Figure 18.

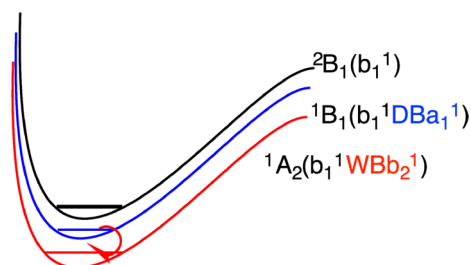


**Figure 18.** Depiction of the nonadiabatic  $a_1$ -to- $b_2$  electronic orbital de-excitation that increases rotational energy within the WBS.

The key observation made in ref 36 to support the existence of this second weakly bound state is that the angular distribution of electrons ejected by a second photon (the first photon excites the anion from its ground state into the  $a_1$  symmetry DBS) is not consistent with detachment from an orbital of  $a_1$  symmetry but is consistent with detachment from an orbital of  $b_2$  symmetry. This

evidence is shown clearly in Figure 3 of ref 36, and those authors suggest that it is a rotational motion that effects the nonadiabatic transition into the orbital of  $b_2$  symmetry from the DBS populated in the first photon-absorption event. When it comes to which rotational levels would be involved, and realizing as was pointed out earlier that  $z$ -axis motion is inoperative, the simple model used in Section III.B.2 can again offer insight. Assuming that the tumbling rotation of the anion can be approximately described in terms of a rigid rotor, its  $j,m$  energy levels are given by eq 24; the electronic energy  $\Delta E'$  resulting from the orbital change must match a  $j \rightarrow j + 1$  rotational energy level spacing  $2(j + 1)b_v$ . This means that states populated by a nonadiabatic conversion of  $\Delta E'$  of electronic energy into rotational energy should have  $j$ -values given by eq 25. Note that, in ref 36, it was not shown definitively that the WBS of  $b_2$  symmetry had an energy below that of the  $a_1$  DBS. In fact, the electronic structure calculations reported in ref 36 place the  $b_2$  state slightly above the  $a_1$  DBS. The energy ordering of the  $a_1$  and  $b_2$  states was inferred from the observation that, although the  $a_1$  DBS had to have been populated by the first photon, by the time the second photon was absorbed the anion had evolved into the  $b_2$  WBS, and this evolution was assumed to have been to a state of lower electronic energy (since rotational motion was needed to induce the nonadiabatic transfer). On the one hand, if this energy ordering is correct, the discussion just offered about Figure 18 would apply, but notice that, in such a nonadiabatic transition, the electronic energy is lowered, but the rotational energy is actually increased, even though rotational motion is involved. On the other hand, if the  $b_2$  WBS of ref 36 had an energy higher than that of the  $a_1$  DBS, then Figure 17 would apply, and population of the  $b_2$  state by a nonadiabatic transition involving rotational motion would consume rotational energy.

#### IV. SUMMARY

A variety of propensity rules resulting from energy, angular momentum, and symmetry conservation arise when electrons are ejected from molecular anions by photon absorption, vibration-induced nonadiabatic energy flow, or rotation-induced energy flow. This work offers an analysis of the similarities and differences that arise when the ejection process consumes energy from a photon, from molecular vibration, or from molecular rotation. The theoretical origins of the propensity rules were treated, and numerous examples were given of their applications to experimental measurements of electron ejection events and the associated angular distributions of the ejected electrons. Special attention was given to detachment from orbitals having very small electron binding energies and thus large radial extent.

#### ■ ASSOCIATED CONTENT

##### Supporting Information

The Supporting Information is available free of charge at <https://pubs.acs.org/doi/10.1021/acs.jpca.0c08016>.

Alternative treatment of the  $A$  factor for photon-induced electron ejection from diffuse orbitals spread over several centers. KE dependence of  $\beta$  for states with very large  $A$  factors. Treatment of non-adiabatic electron ejection rates and angular distributions for vibration-induced electron ejection (PDF)

## AUTHOR INFORMATION

### Corresponding Author

Jack Simons – Henry Eyring Center for Theoretical Chemistry,  
Department of Chemistry, University of Utah, Salt Lake City,  
Utah 84112, United States; [orcid.org/0000-0001-8722-184X](https://orcid.org/0000-0001-8722-184X); Email: [jack.simons@utah.edu](mailto:jack.simons@utah.edu)

Complete contact information is available at:  
<https://pubs.acs.org/10.1021/acs.jpca.0c08016>

### Notes

The author declares no competing financial interest.

## ACKNOWLEDGMENTS

The author thanks Profs. J. R. R. Verlet and A. Sanov for many helpful suggestions and insights.

## REFERENCES

- (1) Sanov, A. Laboratory-Frame Photoelectron Angular Distributions in Anion Photodetachment: Insight into Electronic Structure and Intermolecular Interactions. *Annu. Rev. Phys. Chem.* **2014**, *65*, 341–363.
- (2) Reid, K. L. Photoelectron Angular Distributions. *Annu. Rev. Phys. Chem.* **2003**, *54*, 397–424.
- (3) Oana, C. M.; Krylov, A. I. Cross Sections and Photoelectron Angular Distributions in Photodetachment from Negative Ions Using Equations-of-Motion Coupled-Cluster Dyson Orbitals. *J. Chem. Phys.* **2009**, *131*, 124114.
- (4) Cooper, J.; Zare, R. N. Angular Distributions of Photoelectrons. *J. Chem. Phys.* **1968**, *48*, 942–943.
- (5) Kitsopoulos, T. N.; Waller, I. M.; Loeser, J. G.; Neumark, D. M. High resolution photodetachment spectroscopy of negative ions. *Chem. Phys. Lett.* **1989**, *159*, 300–306.
- (6) Neumark, D. M. Slow Electron Velocity-Map Imaging of Negative Ions: Applications to Spectroscopy and Dynamics. *J. Phys. Chem. A* **2008**, *112*, 13287–13301. Weichman, M. L.; Neumark, D. M. Slow Photoelectron Velocity-Map Imaging of Cryogenically Cooled Anions. *Annu. Rev. Phys. Chem.* **2018**, *69*, 101–124.
- (7) Reed, K. J.; Zimmerman, A. H.; Andersen, H. C.; Brauman, J. I. Cross Sections for Photodetachment of Electrons from Negative Ions Near Threshold. *J. Chem. Phys.* **1976**, *64*, 1368–1375.
- (8) Hanstorp, D.; Bengtsson, C.; Larson, D. J. Angular Distributions in Photodetachment from  $O^-$ . *Phys. Rev. A: At., Mol., Opt. Phys.* **1989**, *40*, 670–675.
- (9) If the orbital from which the electron is detached has d-orbital character, another  $A$  factor arises (see ref 11) and involves the ratio of  $d \rightarrow f$  and  $d \rightarrow p$  radial integrals:  $A_2 * KE = \left| \frac{\kappa_{2,3}}{\kappa_{2,1}} \right|$ . In ref 11 it is shown that, if the d-orbital is formed as a combination of 2p orbital on neighboring atoms, as the  $\pi^*$  orbital of  $O_2$  is,  $A_2$  turns out to be  $\sim 3/5A$ .
- (10) Grumblin, E. R.; Sanov, A. Photoelectron Angular Distributions in Negative-Ion Photodetachment from Mixed sp States. *J. Chem. Phys.* **2011**, *135*, 164302.
- (11) Sanov, A.; Grumblin, E. R.; Goebbert, D. J.; Culberson, L. M. Photodetachment Anisotropy for Mixed s-p States: 8/3 and Other Fractions. *J. Chem. Phys.* **2013**, *138*, 054311.
- (12) Lykke, K. R.; Neumark, D. M.; Andersen, T.; Trapa, V. J.; Lineberger, W. C. Autodetachment Spectroscopy and Dynamics of  $CH_2CN^-$  and  $CD_2CN^-$ . *J. Chem. Phys.* **1987**, *87*, 6842–6853.
- (13) The  $b_2$  orbital of our anion does not contain  $ad_{b_2}$  component, because there is no asymmetry in the total electron distribution to cause such a polarization. However, in Table I I allow for polarization of a  $b_2$  orbital of some other system.
- (14) Wigner, E. P. On the Behavior of Cross Sections Near Thresholds. *Phys. Rev.* **1948**, *73*, 1002–1009.
- (15) Nonadiabatic transitions from an initial electronic state  $\Psi_i$  to a final electronic state  $\Psi_f$  involving a transition from an initial vibration/rotation state to  $\Phi_i$  a final vibration/rotation state is  $\Phi_f$  governed by the

product of two integrals:  $\langle \Psi_f | \nabla | \Psi_i \rangle \bullet \langle \Phi_f | \nabla | \Phi_i \rangle$ . Here, the vector operator  $\nabla$  involves derivatives with respect to the coordinates of the nuclei and can be decomposed into various symmetry-adapted components. Note that  $\frac{\partial}{\partial x}$  has the same symmetry as  $x$  (including the parity symmetry). This material is covered in ref 16 in more detail.

(16) Simons, J. Propensity Rules for Vibration-Induced Electron Detachment of Anions. *J. Am. Chem. Soc.* **1981**, *103*, 3971–3976.

(17) Liu, H.-T.; Ning, C.-G.; Huang, D.-L.; Dau, P. D.; Wang, L.-S. Observations of Mode-Specific Vibrational Autodetachment from Dipole-Bound States of Cold Anions. *Angew. Chem., Int. Ed.* **2013**, *52*, 8976–8979.

(18) Kim, J. B.; Yacovitch, T. I.; Hock, C.; Neumark, D. M. Slow Photoelectron Velocity-Map Imaging Spectroscopy of the Phenoxide and Thiophenoxide Anions. *Phys. Chem. Chem. Phys.* **2011**, *13*, 17378–17383.

(19) Anstötter, C. S.; Mensa-Bonsu, G.; Nag, P.; Rankovic, M.; Kumar T P, R.; Boichenko, A. N.; Bochenkova, A. V.; Fedor, J.; Verlet, J. R. R. Mode-Specific Vibrational Autodetachment Following Excitation of Electronic Resonances by Electrons and Photons. *Phys. Rev. Lett.* **2020**, *124*, 203401.

(20) Anstötter, C. S.; Verlet, J. R. R. Gas-Phase Synthesis and Characterization of Methyl-2,2-dicyanoacetate Anions Using Photoelectron Imaging and Dipole-Bound State Autodetachment. *J. Phys. Chem. Lett.* **2020**, *11*, 6456–6462.

(21) It is worth noting that the workers in ref 20 multiplied the computed IR intensities by a factor that depends on the ejected electron's KE and the electron binding strength as explained in the Supporting Information and as originally explained in ref 16.

(22) Clary, D. C. Photodetachment of Electrons from Dipolar Anions. *J. Phys. Chem.* **1988**, *92*, 3173–3181.

(23) Simons, J. Modified Rotationally Adiabatic Model for Rotational Autoionization of Dipole-Bound Molecular Anions. *J. Chem. Phys.* **1989**, *91*, 6858–6865.

(24) This simplified picture is appropriate given the fact that motion associated with spinning about the Z axis is less important.

(25) See Table 2.4 in Zare, R. N. *Angular Momentum*; John Wiley and Sons, Inc., 1988; ISBN 0-471-85892-7.

(26) This is seen in Figure 7, and the origin and explicit  $J$ -dependence was shown in Chalasinski, G.; Kendall, R. A.; Taylor, H.; Simons, J. Propensity Rules for Vibration–Rotation Induced Electron Detachment of Diatomic Anions: Application to  $NH^- \rightarrow ^N H + e^-$ . *J. Phys. Chem.* **1988**, *92*, 3086–3091.

(27) It will also generate a  $d_{xz}$  wave when acting on the  $p_z$  component of the DBS orbital, but I ignore this for reasons explained earlier.

(28) Edwards, S. T.; Johnson, M. A.; Tully, J. C. Vibrational Fano Resonances in Dipole-Bound Anions. *J. Chem. Phys.* **2012**, *136*, 154305.

(29) Hammer, N. I.; Shin, J.-W.; Headrick, J. M.; Diken, E. G.; Roscioli, J. R.; Weddle, G. H.; Johnson, M. A. How Do Small Water Clusters Bind an Excess Electron? *Science* **2004**, *306*, 675–679.

(30) Rogers, J. P.; Anstötter, C. S.; Verlet, J. R. R. Ultrafast Dynamics of Low-Energy Electron Attachment via a Non-Valence Correlation-Bound State. *Nat. Chem.* **2018**, *10*, 341–346.

(31) Voora, V. K.; Jordan, K. D. Nonvalence Correlation-Bound Anion State of  $C_6F_6$ : Doorway to Low-Energy Electron Capture. *J. Phys. Chem. A* **2014**, *118*, 7201–7205.

(32) Katriel, J.; Davidson, E. R. Asymptotic Behavior of Atomic and Molecular Wave Functions. *Proc. Natl. Acad. Sci. U. S. A.* **1980**, *77*, 4403–4406.

(33) This is certainly true for  $H_2CCN^-$ , but one might imagine a larger anion having vibrational modes of much lower frequency (either due to smaller force constants or/and higher reduced masses). In such cases, it would be possible for a low-frequency vibration of  $b_2$  symmetry to exist and to effect the nonadiabatic transition treated in this case.

(34) Liu, G.; Ciborowski, S. M.; Pitts, D. R.; Graham, D. D.; Buytendyk, A. M.; Lectka, T.; Bowen, K. H. Observation of the Dipole- and Quadrupole-Bound Anions of 1, 4-Dicyanocyclohexane. *Phys. Chem. Chem. Phys.* **2019**, *21*, 18310–18315.

(35) Sommerfeld, T.; Dreux, K. M.; Joshi, R. Excess Electrons Bound to Molecular Systems with a Vanishing Dipole but Large Quadrupole. *J. Phys. Chem. A* **2014**, *118*, 7320–7329.

(36) Yuan, D.-F.; Liu, Y.; Qian, C.-H.; Zhang, Y.-R.; Rubenstein, B. M.; Wang, L.-S. Observation of a  $\pi$ -Type Dipole-Bound State in Molecular Anions. *Phys. Rev. Lett.* **2020**, *125*, 073003.